



**HAL**  
open science

# Monomolecular Mechanisms of Isobutanol Conversion to Butenes Catalyzed by Acidic Zeolites: Alcohol Isomerization as a Key to the Production of Linear Butenes

Monika Gešvandtnerová, Tomáš Bučko, Pascal Raybaud, Céline Chizallet

► **To cite this version:**

Monika Gešvandtnerová, Tomáš Bučko, Pascal Raybaud, Céline Chizallet. Monomolecular Mechanisms of Isobutanol Conversion to Butenes Catalyzed by Acidic Zeolites: Alcohol Isomerization as a Key to the Production of Linear Butenes. *Journal of Catalysis*, 2022, 413, pp.786-802. 10.1016/j.jcat.2022.07.025 . hal-03777822

**HAL Id: hal-03777822**

**<https://ifp.hal.science/hal-03777822>**

Submitted on 15 Sep 2022

**HAL** is a multi-disciplinary open access archive for the deposit and dissemination of scientific research documents, whether they are published or not. The documents may come from teaching and research institutions in France or abroad, or from public or private research centers.

L'archive ouverte pluridisciplinaire **HAL**, est destinée au dépôt et à la diffusion de documents scientifiques de niveau recherche, publiés ou non, émanant des établissements d'enseignement et de recherche français ou étrangers, des laboratoires publics ou privés.

# Monomolecular mechanisms of isobutanol conversion to butenes catalyzed by acidic zeolites: alcohol isomerization as a key to the production of linear butenes

Monika Gešvandtnerová<sup>a</sup>, Tomáš Bučko<sup>a,b</sup>, Pascal Raybaud<sup>c</sup>, Céline Chizallet<sup>c</sup>

<sup>a</sup>*Department of Physical and Theoretical Chemistry, Faculty of Natural Sciences, Comenius University in Bratislava, Mlynská Dolina, SK-84215 Bratislava, SLOVAKIA*

<sup>b</sup>*Institute of Inorganic Chemistry, Slovak Academy of Sciences, Dúbravská cesta 9, SK-84236 Bratislava, SLOVAKIA*

<sup>c</sup>*IFP Energies nouvelles, Rond-Point de l'échangeur de Solaize, BP3, 69360 Solaize, FRANCE*

---

## Abstract

Density functional theory calculations are performed to explore the mechanisms of poorly understood monomolecular conversions of isobutanol to butenes, belonging to an important class of transformations of biobased molecules into chemicals. Except for the lowest reaction temperatures (<405 K), at which a conventional mechanism via alkoxide intermediates dominates, the alkenes formation proceeds via newly explored routes involving alcohol isomerization followed by dehydration according to a E2 mechanism. The carbenium ion deprotonation in the latter step is facilitated by the water molecule created during the reaction. In contrast, the isomerization of alkenes was found to be unfavorable at all reaction conditions. A favourable unconventional mechanism of formation of linear alkenes from isobutanol is discovered, in which the isomerization and dehydration are combined into a single reaction step. Our work represents a key in unraveling why linear butenes are formed in some zeolites when isobutanol is used as the dehydration reagent.

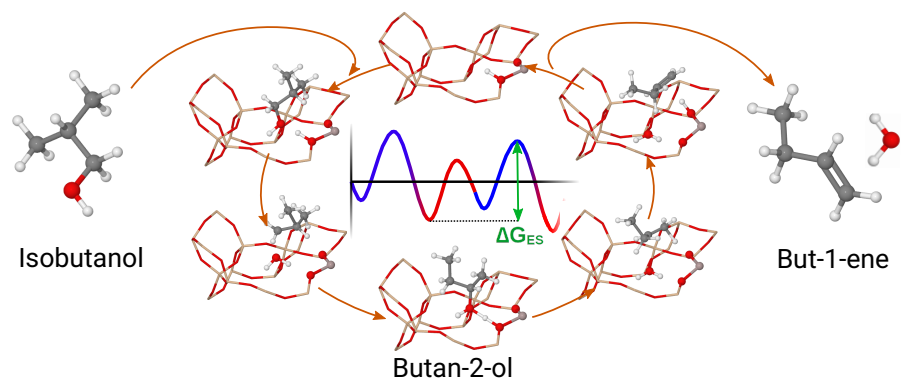
---

*Email addresses: gesvandtnerova2@uniba.sk (Monika Gešvandtnerová), bucko19@uniba.sk (Tomáš Bučko), pascal.raybaud@ifpen.fr (Pascal Raybaud), celine.chizallet@ifpen.fr (Céline Chizallet)*

## Graphical Abstract

**Monomolecular mechanisms of isobutanol conversion to butenes catalyzed by acidic zeolites: alcohol isomerization as a key to the production of linear butenes**

Monika Gešvandtnerová, Tomáš Bučko, Pascal Raybaud, Céline Chizallet



## Highlights

**Monomolecular mechanisms of isobutanol conversion to butenes catalyzed by acidic zeolites: alcohol isomerization as a key to the production of linear butenes**

Monika Gešvandtnerová, Tomáš Bučko, Pascal Raybaud, Céline Chizallet

- Branched and linear alkenes formation proceeds via alcohol isomerizations
- A favourable single-step mechanism for linear butenes formation discovered
- The water molecule created in reaction facilitates the proton transfer
- Direct alkenes isomerization found unfavourable under all reaction conditions

*Keywords:* acidic zeolites, dehydration, isomerization, alcohol, biobutanol, energy span concept, free energy of activation, density functional theory

---

## 1. Introduction

The production of alkenes from alcohols, particularly butanols, is of great importance for the production of chemicals and fuels from renewables [1, 2, 3]. Alcohol reactions are also prototypical models used to estimate the acidity/basicity of various heterogeneous catalysts [4, 5]. Zeolite catalysts are well known for their effectivity and selectivity in the dehydration of butanols to butenes [6] and for the skeletal isomerization of n-butenes to isobutene [7]. The dehydration of butan-1-ol *versus* isobutanol in zeolites is one of the reactions that gave birth to the concept of shape selectivity in the 1960s [8, 9]. However, despite decades of investigation, the transformation mechanisms of butanols in zeolites remain highly debated. In particular, the formation of linear butenes (but-1-ene, *cis*- and *trans*-but-2-enes) *versus* isobutene, depending on the starting alcohol (butan-1-ol, butan-2-ol, isobutanol, tert-butanol, see Figure 1) remains poorly understood. Indeed, whereas alumina produces exclusively the expected isobutene isomer from isobutanol [10, 11, 12], variable yields of linear butenes depending on the particular zeolite topology and operating conditions [13, 10] are obtained with zeolite catalysts.

Two recent experimental studies provided detailed information on isobutanol dehydration in ferrierite catalysts [13, 10]. In both studies, a high selectivity (>80 %) toward linear butenes has been demonstrated. The observed [linear alkenes]/[isobutene] ratio of alkenes formed as products of the isobutanol dehydration was found to be much higher compared to the equilibrium distribution (4.9 [10] and 3.2 [13] at 523 K *versus* 0.7 at equilibrium). These results may seem counterintuitive at first glance, as ferrierite is a very efficient catalyst for the skeletal isomerization of linear butenes to isobutene [14, 15, 16, 17]. Thus, starting from alcohols or directly from the corresponding alkenes, selectivities are fully inverted. A selectivity to linear butenes higher than expected from the

equilibrium distribution was also reported for Theta-1 zeolite [10]. Notably, the quantitative production of linear butenes from isobutanol is not restricted to the case of zeolite catalysts. It was also observed in silica-based mixed oxides [18] for example. Furthermore, starting from butan-1-ol, isobutene can be obtained in zeolites such as Theta-1 and ZSM-23, under conditions in which isomerization of butenes is not expected [19]. Thus, the mechanisms of various skeletal isomers formations upon butanol dehydration deserve detailed deciphering.

Most often, the formation of linear butenes from isobutanol is assigned to *a posteriori* isomerization of alkenes, or of tertiary / secondary carbenium ions that are assumed to be formed as reaction intermediates in the course of dehydration or isomerization of alkenes [20]. However, a comparison of the reactivity of silica-based catalysts in isobutanol dehydration (yielding linear butenes) and isobutene isomerization shows that in similar reaction conditions, the latter is much slower than the former [18]. A similar conclusion was made for the ferrierite zeolite [10]. Thus, *a posteriori* isomerization cannot explain the formation of linear butenes from isobutanol. It was tentatively proposed that isomerization should proceed immediately after the formation of primary carbenium ions from isobutanol, without the formation of isobutene as a primary product [13, 10, 18]. However, it remains unclear why this very unlikely primary carbenium ion should be formed more easily from the alcohol than from the alkene. All the more so as butene isomerization mechanisms, themselves strongly debated, are not expected to take place through primary carbenium ions only, but through alkoxide-based or bimolecular mechanisms [14, 16, 21, 22]. Stabilization of the primary carbenium ion in the form of an alkoxide (observed by infrared spectroscopy and nuclear magnetic resonance at temperatures lower than the reaction temperature [23, 20, 24]), or synchronous dehydration and isomerization reactions [10], have also been proposed to be at the origin of the formation of linear butenes, but evidence still needs to be found for such mechanisms.

Furthermore, Buniazet et al. [13] ruled out ether-mediated mechanisms (in-

termolecular dehydration) to explain the formation of linear butenes, which was based on the fact that the thermal evolution of the selectivity to linear butenes measured experimentally was not found to follow the evolution of the rate of ether formation predicted by density functional theory (DFT) calculations [25]. This absence of ether-mediated mechanism is also corroborated in the case of isobutanol dehydration in ZSM-5, faujasite and mordenite [26, 27]. Van Daele et al. [10] also ruled out a role of carbonaceous deposits in the formation of linear butenes. These results motivate a deeper computational study of the monomolecular dehydration mechanisms of isobutanol that are likely at the core of the linear butene selectivity.

DFT simulation is a very useful tool to address questions related to catalytic mechanisms. It has been instrumental in the elucidation of the reaction mechanisms for short-chain alcohol dehydration into alkenes and ethers catalyzed by zeolites, mainly methanol [28, 29, 30], ethanol [31, 32, 33] and propanols [34]. The case of butanols is more complex due to the isomerization reactions that take place concomitantly, and was much more scarcely addressed by DFT. Recently, John et al. [35, 25] studied the dehydration mechanisms of butan-1-ol in different zeolite catalysts (H-FAU, H-FER, H-ZSM-5, H-ZSM-22) proceeding through monomolecular and bimolecular mechanisms involving ether intermediates. Regarding the monomolecular steps that are relevant within the present context, they compared what they called E1-like, E2 *anti* and *syn* elimination mechanisms, as well as alkoxide-mediated steps. Subsequently, the authors completed the reaction network that included the monomolecular butene isomerization steps needed for the production of but-2-enes and isobutene from butan-1-ol [36, 37]. The formation of isobutene by skeletal isomerization performed through butoxide-mediated mechanisms was considered in the *ab initio* microkinetic modeling. The results confirmed that *a posteriori* skeletal isomerization under dehydration conditions is not a relevant route. Furthermore, the microkinetic modeling demonstrated a strong influence of reaction conditions on the preferred reaction mechanism: a temperature below 400 K was shown to favor ether formation, whereas a higher temperature favored butene

production. Gunst et al. [26] addressed the case of isobutanol dehydration in H-ZSM-5, but only considered the formation of isobutene in their *ab initio* investigation.

In the present work, we explore, by means of periodic density functional theory calculations, the monomolecular mechanisms of transformation of butanols into butenes catalyzed by framework bridging Si-(OH)-Al groups, with the main goal of proposing mechanisms that explain the formation of linear butenes from isobutanol. We chose the chabazite (CHA) model framework as a prototype of zeolite catalyst. This choice has been motivated by the fact that the structure of CHA can be represented by a relatively small unit cell (the supercell for the siliceous form used in this work contains 72 atoms) leading to a significant saving in simulation time as compared to FER with at least 216 atoms. Also, the fact that CHA contains only one type of adsorption cage makes the initial exploration of the mechanisms easier in comparison to FER, in which two channels of distinctly different sizes have to be considered. Since the size of the cage of CHA is relatively large (the maximal diameter of sphere that can be included is  $\sim 7.4$  Å), the energetics computed for different mechanisms is expected to be similar to that of reactions in the larger channel of FER, while the confinement effects are likely to play a certain role when reactions occur in the smaller channel. We use the static approach based on the harmonic oscillator, rigid rotor, and ideal gas approximations to the transition state theory (TST) to account for thermal effects. We used this model, despite its well-known [38, 39] deficiencies, due to its computational efficiency allowing us to rapidly explore a sufficiently large configurational space relevant to transformations discussed in this work. The CPU intense and time consuming accurate free energy calculations requiring an explicit sampling will be performed in our future work of a subset of most relevant reactions identified here. Our calculations suggest that the so far overlooked isomerization of alcohols themselves, preceding dehydration or occurring simultaneously with dehydration, plays a key role in the formation of linear butenes from isobutanol, especially when the isomerization of alkenes is not favored. To the best

of our knowledge, the transformation process of isobutanol to other butanols has never been explored in the context of isobutanol to butenes transformation.

After giving methodological details, we begin our discussion by analyzing the conventional dehydration of butanols to alkenes that does not involve any skeletal isomerization (Section 3.1). Conventional chain of transformations from branched alcohol to linear products via reaction steps involving alkoxide intermediates is discussed in Section 3.2. Alcohol isomerization reactions catalyzed by bridging OH groups are explored in Section 3.3. In Section 3.4, synchronous dehydration and isomerization mechanisms obtained for transformations of isobutanol to but-1-ene and butan-1-ol to but-2-ene are presented. In Section 4, we analyze various possible dehydration routes by means of the energy span concept [40, 41], the effect of temperature on calculated energy spans, and compare the calculated kinetic features with experimental data. Finally, conclusions are given in Section 5.

## 2. Methods

Periodic DFT calculations were performed using the VASP code [42, 43, 44] in version 5.4.4. The Kohn-Sham equations have been solved variationally in a plane-wave basis set using the projector-augmented-wave (PAW) method of Blöchl [45], as adapted by Kresse and Joubert [46]. The PBE exchange-correlation functional in the generalized gradient approximation proposed by Perdew et al. [47] was used. The D2 correction of Grimme [48] as implemented in VASP [49] was applied to account for long-range dispersion interactions.

The structural model of CHA used in the previous theoretical work of Rey et al. [39] has been employed. This model contains 24 tetrahedral sites and one bridging OH group site. To create the bridging OH group, one of the Si atoms of the framework was replaced by an Al atom and a hydrogen atom was initially placed on the oxygen site O1, which, according to experiment [50], represents one of two highly populated acid sites present in CHA. We note that the proton position in zeolite changes within the sequence of elementary steps, as

dictated by the course of the reaction. Since all four Brønsted acid sites that can be formed in CHA are, according to our calculations nearly degenerate energetically (their potential energies differ by less than  $4 \text{ kJ mol}^{-1}$ ) and also their protons are accessible from the adsorption void in a similar way, we do not expect that a different choice of the initial position of the active site should lead to significant modification of computed results. Owing to the relatively large unit cell used in our simulations, the Brillouin zone sampling was restricted to the  $\Gamma$ -point.

Plane wave cutoff energy was set to 400 eV, and the convergence criterion for the SCF cycle was set to  $10^{-6} \text{ eV/cell}$ . Geometric optimizations were stopped when all forces acting on the atoms were smaller than  $0.005 \text{ eV/\AA}$ . Transition states (TS) were optimized using the GADGET optimization engine [51, 52]. Subsequently, potential energy minima representing stable reactant and product states linked with TS through the intrinsic reaction coordinate (IRC) [53, 54] were identified using the damped velocity Verlet algorithm [55]. This procedure, which was strictly followed for each reaction considered in this work, reveals that reactions with structurally similar transition states might be eventually very different in some cases (e.g., cf. the structures of TS for I2 (Fig. S8) and DHI2 (Fig. S9) and the corresponding animations provided as Supporting Material (see Section SI)). Indeed, it is often a subtle structural detail, such as the particular orientation of the cation with respect to the zeolite framework, that decides, e.g., which particular hydrogen is eventually shifted to zeolite or whether or not the water molecule is reattached to a hydrocarbon fragment.

Vibrational analysis was carried out via finite differences to test the stationarity of relaxed structures. To this end, a three-point formula was used with a numerical step of  $0.01 \text{ \AA}$ . When needed, additional line minimizations along undesired unstable modes have been performed until the vibrational eigen-spectra were correct (i.e., with zero and one imaginary frequency for the stable and transition states, respectively).

The calculation of thermodynamic properties has been performed using the harmonic oscillator, rigid rotor, and ideal gas approximations, as described in

Section SIII in Supporting Information. Unless stated otherwise, the simulation temperature of 500 K has been assumed. This choice has been made to correspond to the usual experimental conditions reported in the literature, e.g., in the work of Buniazet et al. [13] (473-548 K) and Van Daele et al. [10] (523 K). A wider temperature interval was chosen for the investigation of the thermal evolution of the energy span. The pressure for the gas phase molecules was set to 101325 Pa. All the computed relative energies discussed in this work have been rounded to  $0.5 \text{ kJ mol}^{-1}$  and, similarly, the computed entropies have been rounded to  $1 \text{ J mol}^{-1} \text{ K}^{-1}$ . In order to avoid significant rounding off errors, however, the rounding has been done after computing differences.

The drawings of the structures and schemes presented in this work were created using the program VESTA [56] and Marvin JS [57], respectively.

### 3. Results

The reaction networks under consideration are illustrated in Fig. 1 and Fig. 2. All computed free energies, enthalpies, entropies, and electronic contribution to free energies of the reactant (R), transition (TS) and product (P) states referenced to the isobutanol molecule in gas phase and a clean CHA zeolite are collected in Table 1 and Table S1. The quantities of activation and of reaction are compiled in Table 2 and Table 3, respectively. For transformations involving alkoxide intermediates these quantities are listed in Table S2 and Table S3, respectively. The computed free energies of the products increase in the order isobutene < *trans*-but-2-ene < *cis*-but-2-ene < but-1-ene, which is in accordance with the relative stabilities of the corresponding gas-phase molecules (see Table S4 in Supporting Information). The reactant, transition state, and product structures for all transformations are shown in Supporting Information (Fig. S5-S13). Some of the reactant, intermediate, or product configurations form multiple rotamers and certain elementary steps start from or lead to specific rotamers (see Section SIV). As discussed in Section SIV, these rotamers are nearly degenerate in energy and separated by potential energy barriers that

are significantly lower than the barriers for the slowest reaction in the sequence of transformation. It is therefore legitimate to consider the transformation between different rotamers of the same molecule as a fast process that can be ignored in the kinetics analyses. The only exception is but-2-ene, where the rotational barrier is very high (353 kJ/mol), which is the reason why we considered its two isomers (*trans* and *cis*) as two different products, as it is also commonly done in the literature [13]. Animations of each elementary step are uploaded as a part of Supporting Information and the list of file names is provided in Section SI of Supporting Information. It is noteworthy to mention that, with the exception of alkoxide-based mechanisms, all activation entropies are positive, indicating that the reactant states of all reaction steps are tighter than the linked transition state involving an essentially unbound water molecule (*vide infra*), as will be shown below. We note that an exactly opposite behavior was observed for hydrocarbon isomerization reactions [39]. Positive activation entropies are, however, documented for alcohol dehydration reactions [58, 59].

### 3.1. Conventional dehydration of alcohols into alkenes

In this section we discuss direct transformations of isobutanol to isobutene (path DH1), tert-butanol to isobutene (path DH2), butan-2-ol to *cis*-but-2-ene and to *trans*-but-2-ene (path DH3-*cis* and DH3-*trans*, respectively), butan-2-ol to but-1-ene (path DH4), and butan-1-ol to but-1-ene (path DH5) catalyzed by the bridging OH group, occurring without any change in the hydrocarbon skeleton. In the context of the E2 variable transition state theory [60], most elimination reactions found here are of E1-type as the C-O bond breaking takes place before C-H bond breaking. However, as no carbenium intermediate is found, they still belong to the E2 family. Schematic representation of the mechanism for the transformation of isobutanol to isobutene (path DH1) is depicted in Fig. 3.

With the exception of the dehydration of tert-butanol into isobutene (DH2, *vide infra*), these transformations proceed via very similar mechanisms: the OH group of the alcohol molecule is protonated by the bridging OH group of the

zeolite, creating thus a H<sub>2</sub>O molecule that detaches from the hydrocarbon moiety, giving rise to a carbenium cation transition state. The latter subsequently deprotonates via the H transfer to a framework oxygen, thus restoring the bridging OH group. This single-step reaction corresponds to a *syn* E2 elimination mechanism [61]. Notably, this mechanism corresponds to what John et al. [35] termed a *syn* elimination (they used the E2 terminology only for the *anti* E2 mechanisms).

Instead of an *anti* E2 mechanism reported in the literature for ZSM-5 [35], we found an E1 mechanism, with a tertiary carbenium ion (tert-butyl cation) as an intermediate. This reaction proceeds in two steps, DH1-anti-a followed by DH1-anti-b, in which the cation deprotonates (see Fig. S5). It is evident from our computed results presented in Table S1 of Supporting Information that transition state for the DH1-anti-b mechanism is energetically very similar to that determined for the *syn* variant (free energy difference of  $\sim 5$  kJ mol<sup>-1</sup> only) and hence one can expect that both alternatives will be kinetically nearly equivalent. For simplicity, we chose the *syn* variant for our kinetics analysis presented in Section 4, but virtually identical results are obtained when the *anti* variant is used instead.

In all dehydration reactions, butenes formed a  $\pi$ -complex on a restored bridging OH group, while the H<sub>2</sub>O molecule created upon dehydration remained nearby the reaction site. Selected geometric features of the transition states are reported in Table 4. In the case of reactions DH1 and DH3-DH5, the breaking C-O bond is close to 2.3 Å for transition states corresponding to primary carbenium ions (isobutanol in DH1 and butan-1-ol in DH5), whereas it is slightly longer for butan-2-ol in DH3-cis, DH3-trans, and DH4 (close to 2.6 Å). The breaking C-H bond restores an O-H bond with a framework oxygen, the length of which tends to increase with the degree of substitution of the carbon atom, although the trend is not strictly monotonous.

The dehydration reactions discussed here are endothermic and also endergonic at 500 K, despite significantly positive reaction entropies explained by the formation of two molecules (alkene plus water) out of one alcohol molecule

(Table 3). Electronic barriers for these reactions (omitting DH2 at this stage) fall into interval between 103.5 (DH3-trans) and 148.5 kJ mol<sup>-1</sup> (DH1) (Table 2). The results obtained for transformations of isobutanol (DH1, 148.5 kJ mol<sup>-1</sup>) and butan-1-ol (DH5, 142.0 kJ mol<sup>-1</sup>) compare well with the values reported in previous theoretical studies for the same reactions catalyzed by ZSM-5 (147 kJ mol<sup>-1</sup> [35] and 139 kJ mol<sup>-1</sup> [26] for isobutanol and butan-1-ol, respectively). As mentioned previously, the activation entropies are positive (between 12 and 39 J mol<sup>-1</sup> K<sup>-1</sup>) for these five elementary steps, indicating that the transition state is actually less constrained than the reactant. In the case of isopropanol dehydration on alumina and silica-alumina models, the activation entropy for E2 monomolecular dehydration reactions turned out to be positive or negative, depending on the kind of mechanism involved [62, 63]. However, the important difference compared to the reactions studied here is that the released water molecule was covalently bound to the Lewis acid site of the catalyst, and hence it could not significantly contribute to the entropy increase.

Of the four alcohol-alkene conversions discussed so far, the highest free energy of activation was found for the transformation of isobutanol to isobutene (133.5 kJ mol<sup>-1</sup>, path DH1). The free energy of the corresponding TS is comparable to that of TS for the path DH5 (Table 1) but significantly higher (by >40 kJ mol<sup>-1</sup>) than the free energies of transition states for the paths DH3-cis, DH3-trans, and DH4. The calculated values of the free energy barriers are indeed 117.5 kJ mol<sup>-1</sup> (path DH5), 98.5 kJ mol<sup>-1</sup> (path DH4), 81.5 kJ mol<sup>-1</sup> (path DH3-cis), and 73.5 kJ mol<sup>-1</sup> (path DH3-trans). A likely reason for these distinctly different stabilities lies in the nature of the carbenium cation transition state: the cation is primary in the DH1 (reactant: isobutanol) and DH5 (reactant: butan-1-ol), whereas it is secondary in the case of the DH3-cis, DH3-trans, and DH4 (reactant: butan-2-ol), as discussed in [11]. As described above, the nature of the carbenium ion is reflected in the length of C-O distance, which is longer for secondary carbenium ions due to the higher stability of the carbenium and the weaker interaction with H<sub>2</sub>O.

For tert-butanol dehydration (DH2), a different water-mediated mechanism

was found (see Fig. 5). As for other DH mechanisms, it starts with the protonation of the OH group of the alcohol molecule, followed by the breaking of the C-O bond and deprotonation of the C-H bond in  $\beta$  position. Unlike in DH1 and DH3-5, this step does not correspond to a direct protonation of a neighboring framework oxygen, but instead is mediated by the water molecule itself. The process of proton transfer via water molecule is known as the Grotthuss mechanism [64, 65]. Hence, the leaving O-H group behaves as the base that captures the proton of the C-H bond. Within the same elementary step (i.e., along a single IRC, see Fig. S14), the hydroxonium ion generated by the protonation of water restitutes a Brønsted acid site on a framework oxygen. This specific mechanism is reflected by the longer  $d_2$  value in Table 4, showing the independence of the C-H bond breaking and H-O bond formation from the framework. In addition, the breaking C-O bond is much longer in DH2 (about 2.9 Å) than that found in other direct dehydration mechanisms, which is likely a consequence of the need for the water molecule to assume a position closer to the H atom of the breaking C-H bond and the tertiary nature of the TS. This mechanism is analogous to the “E1-like” mechanism identified by John et al. [35] for the conversion of butan-1-ol in H-ZSM-5, and resembles the previous proposals made for alumina catalysts on the basis of DFT calculations [66]. Notably, as it is a single step reaction without carbenium intermediate, it may rather be considered to be of *syn* E2 nature [61].

In the case of butan-1-ol in H-ZSM-5, John et al. [35] found that this mechanism was less favorable than other E2 mechanisms. For tert-butanol dehydration in CHA, we were also able to identify the *anti* E1 variant (DH2-anti-a), with the transition state free energy nearly identical to that determined for the reaction DH2 discussed above (see Table S1 in Supporting Information). Nevertheless, the former requires a special orientation of the reactant with respect to Al, achieved by rotating the protonated OH group around the CH<sub>2</sub>-CH axis by about 180 deg. (see state R in Fig. S6). This rotation is an activated process with a barrier that must be at least slightly higher than 68.0 kJ mol<sup>-1</sup>, which is the free energy difference between the initial states of DH2-anti-a and DH2.

Furthermore, the product of DH2-anti-a is, due to the unfavorable position of the water formed upon dehydration with respect to the Al site,  $61.5 \text{ kJ mol}^{-1}$  higher in free energy than the product of DH2. Therefore, we consider the DH2-anti-a variant to be at least slightly less favorable than DH2 and use only the latter in our kinetics analysis presented in Section 4. We emphasize, however, that we do not exclude the DH2-anti-a mechanism and our choice has been made in favor of simplicity of analysis. In fact, replacing the DH2 step by its DH2-anti-a alternative does not lead to any significant variation of our predictions based on the energy span concept.

The free energy barrier for DH2 ( $69.0 \text{ kJ mol}^{-1}$ ) is much lower than that for all other DH reactions (Table 2), both for enthalpic and entropic reasons. Indeed, the formation of a tertiary alcohol leads to a more stable transition state. The entropy gain is also higher ( $43 \text{ J mol}^{-1} \text{ K}^{-1}$ ), suggesting that the structure of the TS is less constrained due to its connection to the framework by a single (OH part) instead of two (OH and HC) moieties in conventional dehydration mechanisms.

We note on passing that we identified a related water-mediated mechanism for the transformation of butan-1-ol to but-1-ene (path DH5w), shown in Fig. 6. In this case, after the detachment of the protonated OH from the molecule, first a primary carbenium cation is formed along the IRC (not as a local energy minimum, see Fig. S14). Then, a proton transfers from the neighboring C atom to form a secondary cation (again, not as a local energy minimum). This isomerization does not appear in any other DH type mechanism. Then, the secondary carbenium deprotonates with the involvement of water, as described for the path DH2. The structure of the transition state corresponds to that of the isomerization process, i.e., the hydride shift transformation of the primary carbenium into the secondary carbenium ion. When comparing the two mechanisms found for the transformation of butan-1-ol to but-1-ene (DH5 versus DH5w), the free energy of TS increases by  $\sim 9 \text{ kJ mol}^{-1}$  (Table 1) in DH5w, and the free energy barrier increases by  $16.5 \text{ kJ mol}^{-1}$  (Table 2) due to differences in the stability of initial configurations for the adsorbed alcohol found from

the two IRCs. Although not similar in nature of the transition state structures, the water-mediated mechanisms (DH2 and DH5w) exhibit the same activation entropy ( $43 \text{ J mol}^{-1} \text{ K}^{-1}$ ), suggesting that the latter is mainly driven by the absence of a direct connection between the leaving H atom (from the C-H bond) and the zeolite framework. Although its product is the one of a direct dehydration reaction, the DH5w reaction is strictly speaking not a direct dehydration mechanism, as it involves a H shift at the same time. As will be shown later, it is more closely related to a synchronous dehydration plus isomerization step, which will lead to unexpected products in cases developed in Section 3.4.

The products created in the DH2 and DH5w paths are  $\pi$ -complexes with water in between, equivalent to a hydroxonium cation (seen as the complex formed by the zeolite proton and the water molecule). Since water interacts effectively with the zeolite framework and the alkene in these complexes, the latter are significantly more stable (by  $\sim 40 \text{ kJ mol}^{-1}$ ) than the  $\pi$ -complexes formed in the conventional paths DH1 and DH5, respectively, where  $\text{H}_2\text{O}$  is only weakly H-bound to zeolite.

### 3.2. Transformations involving alkoxide intermediates and alkene isomerization reactions

As discussed by John et al. [35] for the case of butan-1-ol conversion, one possible mechanism of alcohol dehydration involves the route through alkoxide intermediates. Such a mechanism was also considered in the work of Boronat et al. [21], where the isomerization of but-1-ene was studied. In fact, the whole reaction network discussed so far (Fig. 1) can be modified so as to involve alkoxides (Fig. 2). As discussed by John et al. [35], conversion of alcohol into alkoxide requires a special orientation of the reactant with respect to Al, which is achieved by rotating the protonated OH group around the  $\text{CH}_2\text{-CH}$  axis by about 180 deg. According to our calculations, this rotation proceeds in three steps shown in Fig. S10. The largest free energy barrier in this rotation was obtained for step R-a ( $67.0 \text{ kJ mol}^{-1}$ ), while the subsequent steps (R-b and R-c) involve much smaller free energy barriers of 11.5 and 18.0  $\text{kJ mol}^{-1}$ ,

respectively (see Table S2)

The common first reaction step for all the paths described in this section is the formation of isobutoxide species (path DHA1-a, Fig. S11). Although formally stable, the reactant of this reaction step (rotated and protonated isobutanol) is partly activated, with a free energy of  $44.5 \text{ kJ mol}^{-1}$  higher (Table 1) compared to the reference state, which is isobutanol molecule in the gas phase and a clean zeolite. Consequently, the activation free energy for isobutoxide formation, defined with respect to this high-energy initial state, is very low (only  $63.0 \text{ kJ mol}^{-1}$ ), but the free energy of the corresponding TS is actually  $13\text{-}25 \text{ kJ mol}^{-1}$  higher than that for TS of isobutanol to isobutene (path DH1), isobutanol to tertbutanol (path I1), or isobutanol to butan-2-ol (path I2) conversions discussed in Sections 3.1 and 3.3. Importantly, unlike for the reactions DH1, I1 and I2, the entropy of activation of the path DHA1-a is negative and hence its free energy barrier will increase with temperature. The isobutoxide species can easily undergo a transformation into isobutene while regenerating the zeolite bridging OH group (path DHA1-b, Fig. S11). The TS for the DHA1-b path with a free energy of  $131.0 \text{ kJ mol}^{-1}$  above the reference state is the highest lying state of the entire sequence from isobutanol to isobutene.

To create linear products following an alkoxide-mediated path, isobutoxide must be transformed into secondary butoxide (path IA2-a, see Fig. S11). The TS of IA2-a has the structure of a corner-protonated cyclopropane, with one hydrogen atom replaced by a methyl group (see the TS structure of Fig. S11 (bottom)). Next, the secondary butoxide can be converted into *cis*-but-2-ene, *trans*-but-2-ene, or but-1-ene (paths IA2-b-*cis*, IA2-b-*trans* and IA3-b, respectively, see Fig. S12) via elementary steps with only moderate free energy barriers ( $28.5 \text{ kJ mol}^{-1}$ ,  $63.5 \text{ kJ mol}^{-1}$  and  $47.0 \text{ kJ mol}^{-1}$ , respectively). The highest state for the computed steps of the sequences that link isobutanol to linear alkene products (paths DHA1-a, IA2-a, IA2-b-*cis*, IA2-b-*trans* or IA3-b) is the TS for the path DHA1-a, with free energy being  $107.5 \text{ kJ mol}^{-1}$  above that of the reference state (gas phase isobutanol and clean CHA).

We also considered the transformation of butan-1-ol into n-butoxide (path

DHA5, Fig. S13) discussed also by John et al. [35]. The transition state for this reaction is  $124.5 \text{ kJ mol}^{-1}$  above the reference state, which is to be compared with the values of  $91.0 \text{ kJ mol}^{-1}$ ,  $91.0 \text{ kJ mol}^{-1}$  and  $107.5 \text{ kJ mol}^{-1}$  obtained for the paths DH5, DHI1-cis, and DHI1-trans (see later Sections 3.3 and 3.4), respectively.

Naturally, a subset of transformations shown in Fig. 2 corresponds to alkene isomerization reactions considered also in the literature [36, 37]. In particular, isobutene, formed upon dehydration of isobutanol, can be converted to isobutoxide in reverse DHA1-b mode (-DHA1-b). Subsequently, the latter can be converted to 2-butoxide via IA2-a isomerization step and the linear products can be created via IA2-b-trans, IA2-b-cis, or IA3-b step. As evident from the data presented in Table 1, the free energy barrier for the first step ( $164.5 \text{ kJ mol}^{-1}$ ) is significantly higher than those determined for other reactions from the sequence of transformations leading to linear alkenes (see later Sections 3.3 and 3.4). Furthermore, the free energy of the transition state of this first step is the highest among all reactions considered in this work. As we shall see in Section 4.1, this latter result renders the formation of linear products via alkene transformations very unlikely.

### 3.3. Alcohol isomerization reactions

In this section, we explore the transformation of isobutanol to tert-butanol and butan-2-ol (green arrows in Figure 1) catalyzed by bridging OH groups in CHA, hereafter dubbed as the paths I1 and I2, respectively. Note that direct transformations of isobutanol to butan-1-ol and butan-2-ol to butan-1-ol have been attempted but the corresponding paths have not been identified, since the optimizations converted into the related alcohol to alkene transformation (because carbenium cation created at transition state readily deprotonated before reattachment of temporarily split OH group, see below). Thus, the latter two alternatives appear to be unfeasible.

All relevant reactants, transition states, and products for the I1 and I2 transformations are depicted in Fig. S8. Both reactions start with protonation of the

OH group, after which an essentially neutral water molecule is formed and detached from the newly created carbenium cation. The latter then undergoes a transformation in which the water molecule shifts to the neighbouring C atom, and the H from the tertiary carbon atom is transferred to the terminal CH<sub>3</sub> (path I1, Fig. 7-a) or the CH<sub>3</sub> is shifted from the CH group to the CH<sub>2</sub> group (path I2, Fig. 7-b). According to the IRC analysis, this sequence proceeds in a single step, without passing through any additional local energy minimum (see Fig. S15). The transition state (Table 4) shows a rather loose bonding between the water molecule and the C atoms of the alcohol (breaking the C-O bond of about 2.3 and 2.5 Å, and longer forming the C-O bond at about 3 Å) but a tight bridging bonding between the migrating hydride or methyl group and the same C atoms.

Since breaking the C-H bond is energetically less demanding than that for the C-C bond, the TS of I1 is slightly ( $\sim 10$  kJ mol<sup>-1</sup>) lower in free energy than that of I2 (see Table 1). The calculated free energies of activation are 116.0 kJ mol<sup>-1</sup> (path I1) and 125.0 kJ mol<sup>-1</sup> (path I2) and hence, according to these results, the transformation of isobutanol into tert-butanol should be more facile than the reaction that produces butan-2-ol. Both reactions are exergonic, with nearly identical free energies of reaction ( $\sim -27$  kJ mol<sup>-1</sup>). Interestingly, the products of both transformations are nearly equally stable (free energy difference below 2 kJ mol<sup>-1</sup>) although the enthalpy of tert-butanol is  $\sim 17$  kJ mol<sup>-1</sup> lower than that of butan-2-ol (Table 1). Hence, the latter product is more strongly stabilized by entropy than the former. As a consequence, a similar population of both products is predicted at 500 K, provided that an equilibrium is established in the pore.

Comparing the direct isobutanol dehydration mechanism discussed in Section 3.1 (DH1) with the isobutanol isomerization reactions computed here for the first time, it appears that the free energy barriers of I1 and I2 are both lower than that of DH1. This means that, at 500 K, the *a priori* isomerization of isobutanol is a relevant alternative to direct dehydration discussed in Section 3.1.

### 3.4. Synchronous dehydration and isomerization

In Section 3.1 we assumed conventional routes for the conversion of isobutanol into butenes known from the literature. In these mechanisms, the steps involving the rearrangement of the carbon skeleton (i.e., methyl shift) are strictly separated from the dehydration step. In our exploratory work, however, we also discovered a rather unconventional mechanism, depicted in Fig. 8-a, in which both steps proceed simultaneously, allowing isobutanol to transform into but-1-ene in a single step (path DHI2). Up to the point when the water molecule is created, the new one-step mechanism strongly resembles I2. Unlike in I2, however, the water molecule in DHI2 does not shift from one carbon atom to another, but instead drifts away from the activated complex. A methyl shift occurs concomitantly, with very similar C-C bond distances as found for I2 (Table 4). Similar to DH2 and DH5w, the DHI2 mechanism involves H<sub>2</sub>O as a mediator of the proton transfer from the carbenium cation transition state to framework O, which restores the bridging OH group. It is particularly important that once water is split from the protonated alcohol, it interacts only weakly with the carbenium cation and hence it can assume a position that is very different from that seen in the conventional DH1 mechanism (Fig. 8 and Fig. 3, respectively). This relative independence of the water from the cation manifests itself as a flat region close to the TS on the potential energy profile along IRC (see Fig. S15) which is in striking contrast to that determined for conventional E2 dehydration mechanisms (see Fig. S14). Similarly to other water-mediated mechanisms (DH2 and DH5w), the product created in the DHI2 path is a  $\pi$ -complex formed on the hydroxonium cation and this state is also significantly more stable (by  $\sim 33$  kJ mol<sup>-1</sup>) than the  $\pi$ -complex formed in the conventional path DH4.

A related type of reaction mechanism was found for the transformation of butan-1-ol to but-2-ene (path DHI1-trans and DHI1-cis) shown in Fig. 8-b, where, after protonation of the OH group, H from the nearest CH<sub>2</sub> is shifted to CH<sub>2</sub> from which H<sub>2</sub>O detached. The carbenium cation created in such a way deprotonates to restore the bridging OH group, forming the product *cis*-but-

2-ene (DHI1-cis) or *trans*-but-2-ene (DHI1-trans). As far as the hydrocarbon skeleton is concerned, the structure of the TS (Table 4) resembles that of the TS of path I1, with a slightly more symmetrical position of the bridging H atom. However, the DHI1-cis and DHI1-trans routes were not found to be water-mediated. The transformation leading to *trans*-but-2-ene involves the free energy barrier of  $133.0 \text{ kJ mol}^{-1}$ , which is very similar to the free energy barrier of the DH5w path ( $134.0 \text{ kJ mol}^{-1}$ ), in which but-1-ene is formed from butan-1-ol via a water-mediated mechanism, involving a hydride shift similar to that in DHI1-cis and DHI1-trans.

Thus, thanks to single-step reactions, simultaneously involving both the dehydration and the isomerization processes, we find it is possible to link alcohols to alkenes that are usually considered to be connected by multi-step reactions only. The DHI2 step is particularly interesting in the context of the present study, as it transforms isobutanol directly into linear alkene but-1-ene. The free energy barrier of DHI2 is only  $11 \text{ kJ mol}^{-1}$  higher than that of DH1, but at reverse, the reaction free energy is  $11 \text{ kJ mol}^{-1}$  lower (Table 3). Thus, a deeper analysis, provided in Section 4.1, needs to be performed to conclude about the most favorable routes.

## 4. Discussion

### 4.1. Identification of the preferred dehydration routes

The reaction network considered (Figures 1 and 2) suggests competition between different routes to obtain certain specific products. Three routes are to be considered for the transformation of isobutanol into isobutene, four for isobutanol to but-1-ene and three routes for each of the isobutanol to *cis*-but-2-ene and to *trans*-but-2-ene reactions. To estimate the importance of a given route relative to its alternatives, we use the reaction energy span (ES) concept [40, 41], which is specifically designed to describe catalytic cycles. In this approach, the theoretically determined efficiency of the cycle (in the form of the energy span  $\Delta G_{ES}$ ) can be related to the experimentally obtained turnover frequency (TOF).

The energy span of the cycle can be calculated as  $\Delta G_{ES} = G_{TDTS} - G_{TDI}$  if the TOF-determining transition state (TDTS) appears after the TOF-determining intermediate (TDI) and as  $\Delta G_{ES} = G_{TDTS} - G_{TDI} + \Delta G_{R \rightarrow P}$  if the TDTS appears before TDI. The starting point of the catalytic cycle is the reference reactant state (isobutanol in the gas phase and clean CHA) and the cycle ends by desorption of a specific butene product and water molecule, thus leaving a clean catalyst in the same state as at the beginning of the cycle. The energy span values obtained at 500 K for the reactions considered in this work are compiled in Table 5. The free energies, enthalpies, entropies and electronic contributions to the free energies for desorbed complexes relative to the desorption complex of isobutanol in the gas phase and clean CHA are listed in Table S4.

The direct transformation of isobutanol to isobutene (path DH1) with a free energy barrier of  $133.5 \text{ kJ mol}^{-1}$  can be compared with the two-step process involving either tert-butanol (path I1 followed by path DH2) or primary alkoxide (a five-step process involving three isobutanol rotation steps R-a, R-b, R-c, followed by paths DHA1-a and DHA1-b), as shown in Fig. 9. Within the transformation of isobutanol to isobutene through the sequence I1 + DH2, the isobutanol to tert-butanol (path I1) is identified as the step with the highest free energy of the transition state relative to the reference reactant state ( $82.5 \text{ kJ mol}^{-1}$ ). This TS is identified as TDTS and tert-butanol as TDI, giving rise to an energy span of  $116.0 \text{ kJ mol}^{-1}$ . For the R-a, R-b, R-c, DHA1-a, and DHA1-b sequence, the transition state free energies of the DHA1-a and DHA1-b paths are significantly higher than those of the alternative reactions and the energy span is as large as  $170.5 \text{ kJ mol}^{-1}$ , making the alkoxide route very unlikely compared to its alternatives at 500 K. Hence, we conclude that the two-step mechanism via tert-butanol is clearly kinetically preferred within the energy span formalism. This is an unexpected result, as isobutene is believed to be produced from isobutanol via a simple direct dehydration route, which is not the case. We are not aware of any experiment revealing tert-butanol to be the intermediate for isobutanol dehydration into isobutene, but considering its low dehydration barrier compared to that of isobutanol, it is likely that its concentration will be

very low.

Next, we estimate the importance of the direct transformation of isobutanol to but-1-ene (path DH12) relative to the four-step sequence of elementary steps DH1, -DHA1-b, IA2-a, and IA3-b, the two-step process consisting of isobutanol isomerization into butan-2-ol followed by dehydration of the latter (involving paths I2 and DH4), and the six-step process involving alkoxide intermediates (steps R-a, R-b, R-c, DHA1-a, IA2-a, and IA3-b). As shown in Fig. 10, the two-step transformation with  $\Delta G_{ES}$  of  $128.5 \text{ kJ mol}^{-1}$  is predicted to be more favorable by the energy span model [40, 41] than the direct ( $\Delta G_{ES}$  of  $144.5 \text{ kJ mol}^{-1}$ ), six-step ( $147.0 \text{ kJ mol}^{-1}$ ) or four-step ( $170.5 \text{ kJ mol}^{-1}$ ) alternatives.

Finally, the transformations of isobutanol to *cis*-but-2-ene and *trans*-but-2-ene via dehydration of isobutanol and subsequent isobutene isomerization (paths DH1, -DHA1-b, IA2-a, and IA2-b-*trans* or IA2-b-*cis*), butan-2-ol (paths I2 followed by DH3-*cis* or DH3-*trans*) or via alkoxide intermediates (steps R-a, R-b, R-c, DHA1-a, IA2-a and IA2-b-*cis* (Fig. 11) or IA2-b-*trans* (Fig. 12)) are compared. Because the sequences that produce *cis*-but-2-ene and *trans*-but-2-ene always differ only in the final step, which does not involve TDTS nor TDI, the energy spans ( $170.5 \text{ kJ mol}^{-1}$ ,  $125.0 \text{ kJ mol}^{-1}$  and  $147.0 \text{ kJ mol}^{-1}$  for the four-, two-, and six-step mechanisms, respectively) are, in this case, independent of product. Therefore, in either case, the two-step reaction route is clearly the most favorable, with the energy span being  $\sim 22 \text{ kJ mol}^{-1}$  lower than the alternatives.

#### 4.2. Effect of temperature on energy span

It is clear from the significant differences between the activation entropies determined for the individual elementary steps of different reaction pathways that temperature will affect the preferred reaction mechanism. In this section we, therefore, analyze the temperature dependence of the energy spans. The range of temperatures for this analysis has been chosen to correspond to the interval between the lowest  $T$  at which the given reaction is exergonic (rounded to 5 K) and 900 K. Therefore, the lower  $T$  limit is reaction dependent. Cal-

culations were carried out with an increment of  $\Delta T = 5$  K. As evident from Figs. S16-S19, two types of energy span changes with  $T$  are observed: linear increases or decreases due to explicit dependence of  $\Delta G$  of each state on  $T$ , and variations due to temperature-induced changes in TDTS and/or TDI. The latter manifest themselves as discontinuous changes in slopes of  $\Delta G_{ES}$  versus  $T$  dependencies. For brevity, we focus here on the main thermally induced changes in the preferred reaction mechanisms; a detailed description of  $\Delta G_{ES}$  versus  $T$  trends for each reaction mechanism is discussed in Section SVII (Supporting Information).

For isobutene formation, the most favorable low-temperature (240-330 K) mechanism is the one-step mechanism, while at higher  $T$  ( $>330$  K) the two-step mechanism via alcohol isomerization dominates. The preferred mechanisms for but-1-ene formation for low (350-405 K) and high ( $>405$  K) temperatures are the alkoxide-involving mechanism and the two-step mechanism proceeding through alcohol isomerization, respectively. Qualitatively similar conclusions can also be made for the formation of but-2-enes; only the  $T$  range dominated by the alkoxide-involving mechanism is somewhat shifted (285-350 K and 255-330 K for *cis* and *trans* isomers, respectively). The reaction paths involving alkene isomerizations after the formation of isobutene turned out to be unlikely at all conditions discussed here, which is evident from the fact that the corresponding energy span is always at least  $\sim 20$  kJ mol<sup>-1</sup> higher than that for the dominant reaction mechanism (see Section SVII in Supplementary Information).

Fig. 13 is a graphical summary of  $\Delta G_{ES}$  determined for the most favorable mechanisms for each product considered. At all temperatures, the reaction with the lowest energy span is isobutene formation followed by that producing but-2-enes (the reactions that produce *cis*-but-2-ene and *trans*-but-2-ene have identical energy spans at  $T \geq 450$  K), and but-1-ene (which, however, has the same energy span as other linear products at  $T \geq 530$  K). Notably, the energy spans tend to decrease with temperature up to the point ( $\sim 650$  K) where the desorbed reactant becomes TDI (see Section SVII in Supplementary Informa-

tion). Since the isobutanol adsorption is endergonic from this point on, this regime is rather unfavorable for the transformations discussed here.

#### 4.3. Comparison with experiments

The first fruitful comparison to be made concerns the possibility to form linear alkenes from isobutanol in conditions where alkene isomerization is very slow, thanks to alcohol isomerization reactions that we find.

To go more into details, in H-ZSM-5 at 503 K, isobutanol has been experimentally shown to exhibit lower conversion levels than butan-2-ol [26], which is in line with our computed activation free energy values. However, butan-1-ol was shown to be more reactive than isobutanol and butan-2-ol [26], while the height of the free energy barrier for butan-1-ol that we determined is between that of butan-2-ol and isobutanol. This result suggests that either topology effects play a role (comparing MFI and CHA structure type), or that the direct dehydration pathway is not sufficient to explain respective reactivities.

From the comparison of the energy spans for all isobutanol to alkene transformations (Table 5), the formation of isobutene turns out to be the most favorable, followed by *trans*-but-2-ene and *cis*-but-2-ene, and but-1-ene, which closely correlates with the order of the stability of products in the gas phase (see Table S4) as well as in the zeolite. This result is not in perfect agreement with experimental observations [13, 10] made for the ferrierite zeolite, reporting a higher selectivity toward linear products (19 % of isobutene, 19 % of but-1-ene, and 37 % of *trans*-but-2-ene and 25 % of *cis*-but-2-ene). This discrepancy may prompt future investigations involving topology effects (FER versus CHA).

To go further in deciphering the sources of discrepancy between our calculations and the experimental data, we may compare our calculated activation enthalpies (Table 2) with the experimental results reported by Buniazet et al. [13], which are 101 kJ mol<sup>-1</sup> and 112 kJ mol<sup>-1</sup> for a feed without and with water, respectively. We obtained activation enthalpies ranging between 90.0 kJ mol<sup>-1</sup> and 160.0 kJ mol<sup>-1</sup>, where the highest values belong to reactions in which water was involved in proton mediation. Our results are thus in reason-

able qualitative agreement with the experiment. However, taking into account the two-step process I1 + DH2, and considering the enthalpic components instead of the free energy, one finds an enthalpy span as high as  $136.5 \text{ kJ mol}^{-1}$ . This reveals that further efforts are also needed in the quantitative estimation of both enthalpic and entropic components for the reactions investigated in the present work.

Notably, the experimental distribution suggests that the difference in free energy between different products with the highest and lowest population is only  $\sim 3 \text{ kJ mol}^{-1}$ . Reaching such a resolution by a density functional theory approach is a challenge. First, the static approach free energy results suffer from a significantly large uncertainty which can be best seen by comparing the results for the same state created in different reaction steps. The relative free energy of butan-2-ol calculated with respect to isobutanol, for instance, which is formed as a product in path I2 or reactant in paths DH3 and DH4 ranges from  $-20$  to  $+10 \text{ kJ mol}^{-1}$ . A similar problem with the static approach has also been reported in the previous work of Rey et al. [39]. This problem can be solved by using an explicit sampling method such as molecular dynamics or Monte Carlo simulations. Second, the density functional approximation in itself brings in a significant systematic error due to an approximate treatment of exchange and correlation energy. This fact is evident, e.g., from the comparison of measured and computed thermodynamic data of relevant gas phase molecules presented in Table S5. Thus, in addition to performing *ab initio* molecular dynamics, it will also be necessary to test the predictions against variations in the DFT method. To this end, the recently introduced MLPT approach [67, 68, 69, 70] will be instrumental.

## 5. Conclusions

Monomolecular transformations of isobutanol to butanols and butenes in chabazite at various temperatures have been explored by density functional theory with the goal of explaining the formation of linear butenes starting from

isobutanol. We considered various reaction paths catalyzed by bridging OH groups, involving carbenium cations and alkoxide intermediates. The latter appeared to be much less likely than the direct isomerization and E2 elimination mechanisms. The transformation routes to all main products, including isobutene, but-1-ene, and *cis*- and *trans*-but-2-ene have been identified. In addition to conventional dehydration mechanisms, we have revealed alcohol isomerization mechanisms, and synchronous dehydration and isomerization reactions. These are able to explain the production of linear butenes from isobutanol, without invoking *a posteriori* butene isomerization reactions that are, according to our results, very unlikely under the dehydration operating conditions. The analysis of the effect of temperature on calculated energy spans shows the importance of alcohol isomerization reactions, as they are involved in preferred mechanisms.

We have also shown how the water molecule created in the course of the reaction can mediate proton transfer from the bridging OH group to the alcohol molecule or from the carbenium cation to the zeolite framework to restore the bridging OH group and how its presence leads to a strong stabilization of  $\pi$ -complexes of alkenes formed as products. This behavior opens up alternative reaction mechanisms, in which isobutanol can transform into both branched and linear alkenes in a single reaction step, i.e., without proceeding via a preliminary transformation to linear alcohols, nor via butene isomerization, as was originally expected. As an example of such a direct transformation, the formation of but-1-ene from isobutanol was presented. We also wish to point out that water created as a product of all alcohol to alkene conversions is likely to accumulate in zeolite to some extent. One can therefore not exclude that one or more water molecules are in contact with reactant molecule at any stage of reaction, increasing thus the importance of water mediated mechanisms further. The possible variations of reaction mechanisms due to this effect should be addressed in future works.

Although we succeeded to identify the numerous reaction mechanisms (some of which are, to the best of our knowledge, reported here for the first time), our

results clearly showed that an accurate treatment of thermal effects will be absolutely crucial in the future to improve the quantitative agreement with experiment. This is particularly challenging because the experimentally observed distribution of products suggests only minimal differences ( $\sim 3 \text{ kJ mol}^{-1}$ ) in their relative free energies. To this end, topology effects, dynamic effects (in particular, to assess the role of water on kinetics), and improved level of theory used in quantum-mechanical calculations are to be addressed. Finally, we notice that, due to practical reasons, we have made a number of simplifying assumptions regarding some factors which might also have a certain effect on kinetics of butanols to alkenes transformations. These include (i) neglect of a possible co-adsorption of reactant and product molecules, (ii) neglect of the role of diffusion on reaction kinetics, (iii) role of defects and external surfaces. Each of these effects deserves a dedicated computational study - here we only wish to briefly comment on their possible importance. In the case of (i) one can expect a strongest effect to arise from the competition of alcohol and alkene molecules for the active sites and from the interactions between the reactant and product molecules. Since the interaction of the former with the acid site is significantly (by  $\sim 20 \text{ kJ mol}^{-1}$ ) stronger, this effect will be probably only modest. Assuming that the OH group of alcohol is blocked by the interaction with the acid site, the interaction between alcohol and alkene will be weak and is unlikely to affect the reaction mechanism very significantly. In contrast, the water co-adsorption can, as discussed above, increase importance of mediated proton transfer and we suspect this effect to play important role. As to the point (ii), most of the elementary steps discussed in this work begin and end in a relatively strongly bound state and hence, in principle, all the reaction steps could occur in the vicinity of the same active site. Diffusion, however, is likely to disfavor slowly diffusing products provided a local equilibrium between different alkenes is established in the catalyst, as suggested in recent experimental [10] and computational work [71]. Finally, this work considered bridging OH groups formed in the bulk as the active sites. Some of the very recent experimental studies suggest that the reactions could be actually catalyzed by

the sites located at external surfaces [10]. Most of the mechanisms discussed in this work could be directly applied also to reactions catalyzed by other kinds of surface groups, including silanols, aluminols and Al-(H<sub>2</sub>O) species [72], although significant changes in some of the activation energies could be expected since these sites are less acidic compared to bridging OH sites [73, 74, 75]. In contrast, the involvement of defects or extra-framework aluminum could lead to significant changes in reaction mechanisms elucidation of which would require a further research effort. However, the experimental evidence [10] available as of today suggests that Brønsted rather than Lewis sites are active in alcohol to alkene transformations in zeolites.

## 6. Acknowledgments

Sylvie Maury (IFP Energies nouvelles) is warmly acknowledged for fruitful discussions. MG and TB acknowledge support from IFP Energies nouvelles within the project "Ab initio Molecular Dynamics Investigation of the Reactivity of Zeolites" and from the Slovak Research and Development Agency under the contracts No. VEGA-1/0777/19 and APVV-20-0127.

## References

- [1] N. Savage, Fuel options: The ideal biofuel, *Nature* 474 (2011) S9–11, <https://doi.org/10.1038/474S09a>.
- [2] M. Mascal, Chemicals from biobutanol: technologies and markets, *Biofuels Bioprod. Biorefining* 6 (4) (2012) 483–493, <https://doi.org/10.1002/bbb.1328>.
- [3] P. C. A. Bruijninx, B. M. Weckhuysen, Shale gas revolution: An opportunity for the production of biobased chemicals?, *Angew. Chem. Int. Ed.* 52 (46) (2013) 11980–11987, <https://doi.org/10.1002/anie.201305058>.
- [4] H. Lauron-Pernot, Evaluation of surface acido-basic properties of inorganic-based solids by model catalytic alcohol reaction networks, *Catal. Rev.-Sci. Eng.* 48 (3) (2006) 315–361, <https://doi.org/10.1080/01614940600816634>.
- [5] M. Guisnet, L. Pinard, Characterization of acid-base catalysts through model reactions, *Catal. Rev.-Sci. Eng.* 60 (3) (2018) 337–436, <https://doi.org/10.1080/01614940.2018.1446683>.
- [6] S. Jeong, H. Kim, J. Bae, D. H. Kim, C. H. Peden, Y.-K. Park, J.-K. Jeon, Synthesis of butenes through 2-butanol dehydration over mesoporous materials produced from ferrierite, *Catal. Today* 185 (1) (2012) 191–197, *Catalysis on Energy and Environmental Technologies: 13th Korea-Japan Symposium on Catalysis*.
- [7] G. Seo, S.-H. Park, J.-H. Kim, The reversible skeletal isomerization between n-butenes and iso-butene over solid acid catalysts, *Catal. Today* 44 (1) (1998) 215–222, [https://doi.org/10.1016/S0920-5861\(98\)00193-X](https://doi.org/10.1016/S0920-5861(98)00193-X).
- [8] P. B. Weisz, V. J. Frillette, Intracrystalline and molecular-shape-selective catalysis by zeolite salts, *J. Phys. Chem.* 64 (3) (1960) 382–382, <https://doi.org/10.1021/j100832a513>.

- [9] P. Weisz, V. Frilette, R. Maatman, E. Mower, Catalysis by crystalline aluminosilicates II. Molecular-shape selective reactions, *J. Catal.* 1 (4) (1962) 307–312, [https://doi.org/10.1016/0021-9517\(62\)90058-1](https://doi.org/10.1016/0021-9517(62)90058-1).
- [10] S. Van Daele, D. Minoux, N. Nesterenko, S. Maury, V. Coupard, V. Valtchev, A. Travert, J.-P. Gilson, A highly selective FER-based catalyst to produce n-butenes from isobutanol, *Appl. Catal. B.* 284 (2021) 119699, <https://doi.org/10.1016/j.apcatb.2020.119699>.
- [11] H. Knözinger, H. Bühl, K. Kochloefl, The dehydration of alcohols on alumina: XIV. Reactivity and mechanism, *J. Catal.* 24 (1) (1972) 57–68, [https://doi.org/10.1016/0021-9517\(72\)90007-3](https://doi.org/10.1016/0021-9517(72)90007-3).
- [12] J. D. Taylor, M. M. Jenni, M. W. Peters, Dehydration of fermented isobutanol for the production of renewable chemicals and fuels, *Top. Catal.* 53 (15) (2010) 1224–1230, <https://doi.org/10.1007/s11244-010-9567-8>.
- [13] Z. Buniazet, A. Cabiac, S. Maury, D. Bianchi, S. Loridant, Unexpected selectivity of ferrierite for the conversion of isobutanol to linear butenes and water effects, *Appl. Catal. B.* 243 (2019) 594–603, <https://doi.org/10.1016/j.apcatb.2018.11.007>.
- [14] L. Domokos, L. Lefferts, K. Seshan, J. Lercher, Isomerization of linear butenes to iso-butene over medium pore zeolites: I. Kinetic aspects of the reaction over H-FER, *J. Catal.* 197 (1) (2001) 68–80, <https://doi.org/10.1006/jcat.2000.3056>.
- [15] W. Liu, H. Hu, Y. Liu, L. Zhang, C. Xia, Q. Wang, M. Ke, Distribution of effective ferrierite active sites for skeletal isomerization of n-butene to isobutene, *ChemistrySelect* 4 (27) (2019) 7851–7857, <https://doi.org/10.1002/slct.201901495>.
- [16] H. Mooiweer, K. de Jong, B. Kraushaar-Czarnetzki, W. Stork, B. Krutzen, Skeletal isomerisation of olefins with the zeolite ferrierite as catalyst, in:

- J. Weitkamp, H. Karge, H. Pfeifer, W. Hölderich (Eds.), *Zeolites and Related Microporous Materials: State of the Art 1994 - Proceedings of the 10th International Zeolite Conference, Garmisch-Partenkirchen, Germany, 17-22 July 1994*, Vol. 84 of *Studies in Surface Science and Catalysis*, Elsevier, 1994, pp. 2327–2334, [https://doi.org/10.1016/S0167-2991\(08\)63797-0](https://doi.org/10.1016/S0167-2991(08)63797-0).
- [17] P. Mériaudeau, V. Tuan, N. Le, G. Szabo, Selective isomerization of n-butene into isobutene over deactivated H-ferrierite catalyst: Further investigations, *J. Catal.* 169 (1) (1997) 397–399, <https://doi.org/10.1006/jcat.1997.1656>.
- [18] N. Kotsarenko, L. Malysheva, Influence of the chemical composition of oxide catalysts on the rate of dehydration of isobutanol and the composition of the products formed, *Kinet. Catal.* 24 (1983) 877–882.
- [19] D. Zhang, R. Al-Hajri, S. A. I. Barri, D. Chadwick, One-step dehydration and isomerisation of n-butanol to iso-butene over zeolite catalysts, *Chem. Commun.* 46 (2010) 4088–4090, <https://doi.org/10.1039/C002240C>.
- [20] A. G. Stepanov, K. I. Zamaraev,  $^{13}\text{C}$  solid state NMR evidence for the existence of isobutyl carbenium ion in the reaction of isobutyl alcohol dehydration in H-ZSM-5 zeolite, *Catal. Lett.* 19 (1993) 153–158, <https://doi.org/10.1007/BF00771750>.
- [21] M. Boronat, P. Viruela, A. Corma, The skeletal isomerization of but-1-ene catalyzed by theta-1 zeolite, *Phys. Chem. Chem. Phys.* 3 (2001) 3235–3239, <https://doi.org/10.1039/B103429B>.
- [22] B. de Ménorval, P. Ayrault, N. Gnep, M. Guisnet, Mechanism of n-butene skeletal isomerization over HFER zeolites: a new proposal, *J. Catal.* 230 (1) (2005) 38–51, <https://doi.org/10.1016/j.jcat.2004.09.021>.
- [23] A. G. Stepanov, V. N. Romannikov, K. I. Zamaraev,  $^{13}\text{C}$  CP/MAS NMR study of isobutyl alcohol dehydration on H-ZSM-5 zeolite. Evidence for

- the formation of stable isobutyl silyl ether intermediate, *Catal. Lett.* 13 (1992) 395–405, <https://doi.org/10.1007/BF00765043>.
- [24] K. I. Zamaraev, J. M. Thomas, Structural and mechanistic aspects of the dehydration of isomeric butyl alcohols over porous aluminosilicate acid catalysts, Vol. 41 of *Advances in Catalysis*, Academic Press, 1996, pp. 335–358, [https://doi.org/10.1016/S0360-0564\(08\)60043-7](https://doi.org/10.1016/S0360-0564(08)60043-7).
- [25] M. John, K. Alexopoulos, M.-F. Reyniers, G. B. Marin, First-principles kinetic study on the effect of the zeolite framework on 1-butanol dehydration, *ACS Catal.* 6 (7) (2016) 4081–4094, <https://doi.org/10.1021/acscatal.6b00708>.
- [26] D. Gunst, K. Alexopoulos, K. Van Der Borght, M. John, V. Galvita, M.-F. Reyniers, A. Verberckmoes, Study of butanol conversion to butenes over H-ZSM-5: Effect of chemical structure on activity, selectivity and reaction pathways, *Appl. Catal. A-Gen.* 539 (2017) 1–12, <https://doi.org/10.1016/j.apcata.2017.03.036>.
- [27] A. de Reviere, D. Gunst, M. K. Sabbe, M.-F. Reyniers, A. Verberckmoes, Dehydration of butanol towards butenes over MFI, FAU and MOR: influence of zeolite topology, *Catal. Sci. Technol.* 11 (2021) 2540–2559, <https://doi.org/10.1039/D0CY02366C>.
- [28] P. Huber, F. Studt, P. N. Plessow, Reactivity of surface Lewis and Brønsted acid sites in zeolite catalysis: A computational case study of DME synthesis using H-SSZ-13, *J. Phys. Chem. C* 126 (13) (2022) 5896–5905, <https://doi.org/10.1021/acs.jpcc.2c00668>.
- [29] J. R. Di Iorio, A. J. Hoffman, C. T. Nimlos, S. Nystrom, D. Hibbitts, R. Gounder, Mechanistic origins of the high-pressure inhibition of methanol dehydration rates in small-pore acidic zeolites, *J. Catal.* 380 (2019) 161–177, <https://doi.org/10.1016/j.jcat.2019.10.012>.

- [30] A. J. Hoffman, J. S. Bates, J. R. Di Iorio, S. V. Nystrom, C. T. Nimlos, R. Gounder, D. Hibbitts, Rigid arrangements of ionic charge in zeolite frameworks conferred by specific aluminum distributions preferentially stabilize alkanol dehydration transition states, *Angew. Chem. Int. Ed.* 59 (42) (2020) 18686–18694, <https://doi.org/10.1002/anie.202007790>.
- [31] H. Xia, Monomolecular dehydration of ethanol into ethylene over H-MOR studied by density functional theory, *ACS Omega* 5 (17) (2020) 9707–9713, <https://doi.org/10.1021/acsomega.9b03984>.
- [32] S. Kim, D. J. Robichaud, G. T. Beckham, R. S. Paton, M. R. Nimlos, Ethanol dehydration in HZSM-5 studied by density functional theory: Evidence for a concerted process, *J. Phys. Chem. A* 119 (15) (2015) 3604–3614, <https://doi.org/10.1021/jp513024z>.
- [33] K. Alexopoulos, M. John, K. Van der Borcht, V. Galvita, M.-F. Reyniers, G. B. Marin, DFT-based microkinetic modeling of ethanol dehydration in H-ZSM-5, *J. Catal.* 339 (2016) 173–185, <https://doi.org/10.1016/j.jcat.2016.04.020>.
- [34] Y. Zhi, H. Shi, L. Mu, Y. Liu, D. Mei, D. M. Camaioni, J. A. Lercher, Dehydration pathways of 1-propanol on HZSM-5 in the presence and absence of water, *J. Am. Chem. Soc.* 137 (50) (2015) 15781–15794, <https://doi.org/10.1021/jacs.5b09107>.
- [35] M. John, K. Alexopoulos, M.-F. Reyniers, G. B. Marin, Reaction path analysis for 1-butanol dehydration in H-ZSM-5 zeolite: Ab initio and microkinetic modeling, *J. Catal.* 330 (2015) 28–45, <https://doi.org/10.1016/j.jcat.2015.07.005>.
- [36] M. John, K. Alexopoulos, M.-F. Reyniers, G. B. Marin, Mechanistic insights into the formation of butene isomers from 1-butanol in H-ZSM-5: DFT based microkinetic modelling, *Catal. Sci. Technol.* 7 (2017) 1055–1072, <https://doi.org/10.1039/C6CY02474B>.

- [37] M. John, K. Alexopoulos, M.-F. Reyniers, G. B. Marin, Effect of zeolite confinement on the conversion of 1-butanol to butene isomers: mechanistic insights from DFT based microkinetic modelling, *Catal. Sci. Technol.* 7 (2017) 2978–2997, <https://doi.org/10.1039/C7CY00536A>.
- [38] T. Bučko, L. Benco, J. Hafner, J. G. Ángyán, Monomolecular cracking of propane over acidic chabazite: An ab initio molecular dynamics and transition path sampling study, *J. Catal.* 279 (1) (2011) 220–228.
- [39] J. Rey, A. Gomez, P. Raybaud, C. Chizallet, T. Bučko, On the origin of the difference between type A and type B skeletal isomerization of alkenes catalyzed by zeolites: The crucial input of ab initio molecular dynamics, *J. Catal.* 373 (2019) 361–373, <https://doi.org/10.1016/j.jcat.2019.04.014>.
- [40] S. Kozuch, S. Shaik, How to conceptualize catalytic cycles? The energetic span model, *Acc. Chem. Res.* 44 (2) (2011) 101–110, <https://doi.org/10.1021/ar1000956>.
- [41] C. Amatore, A. Jutand, Mechanistic and kinetic studies of palladium catalytic systems, *J. Organomet. Chem.* 576 (1) (1999) 254–278, [https://doi.org/10.1016/S0022-328X\(98\)01063-8](https://doi.org/10.1016/S0022-328X(98)01063-8).
- [42] G. Kresse, J. Hafner, Ab initio molecular dynamics for liquid metals, *Phys. Rev. B* 47 (1993) 558–561, <https://doi.org/10.1103/PhysRevB.47.558>.
- [43] G. Kresse, J. Hafner, Ab-initio molecular-dynamics simulation of the liquid-metal amorphous-semiconductor transition in germanium, *Phys. Rev. B* 49 (20) (1994) 14251–14269, <https://doi.org/10.1103/PhysRevB.49.14251>.
- [44] G. Kresse, J. Furthmüller, Efficient iterative schemes for ab initio total-energy calculations using a plane-wave basis set, *Phys. Rev. B* 54 (16) (1996) 11169–11186, <https://doi.org/10.1103/PhysRevB.54.11169>.
- [45] P. E. Blochl, Projector augmented-wave method, *Phys. Rev. B* 50 (24) (1994) 17953–17979, <https://doi.org/10.1103/PhysRevB.50.17953>.

- [46] G. Kresse, D. Joubert, From ultrasoft pseudopotentials to the projector augmented-wave method, *Phys. Rev. B* 59 (3) (1999) 1758–1775, <https://doi.org/10.1103/PhysRevB.59.1758>.
- [47] J. P. Perdew, K. Burke, M. Ernzerhof, Generalized gradient approximation made simple, *Phys. Rev. Lett.* 77 (18) (1996) 3865–3868, <https://doi.org/10.1103/PhysRevLett.77.3865>.
- [48] S. Grimme, Semiempirical GGA-type density functional constructed with a long-range dispersion correction, *J. Comput. Chem.* 27 (15) (2006) 1787–1799, <https://doi.org/10.1002/jcc.20495>.
- [49] T. Bučko, J. Hafner, S. Lebégue, J. G. Ángyán, Improved description of the structure of molecular and layered crystals: Ab initio DFT calculations with van der Waals corrections, *J. Phys. Chem. A* 114 (43) (2010) 11814–11824, <https://doi.org/10.1021/jp106469x>.
- [50] L. Smith, A. Davidson, A. Cheetham, A neutron diffraction and infrared spectroscopy study of the acid form of the aluminosilicate zeolite, chabazite (H-SSZ-13), *Catal. Lett.* 49 (3) (1997) 143–146, <https://doi.org/10.1023/a:1019097019846>.
- [51] T. Bučko, J. Hafner, J. G. Ángyán, Geometry optimization of periodic systems using internal coordinates, *J. Chem. Phys.* 122 (12) (2005) 124508, <https://doi.org/10.1063/1.1864932>.
- [52] T. Bučko, Transition state optimization of periodic systems using delocalized internal coordinates, *Theor. Chem. Acc.* 137 (12) (2018) 164, <https://doi.org/10.1007/s00214-018-2367-0>.
- [53] K. Fukui, Formulation of the reaction coordinate, *J. Phys. Chem.* 74 (23) (1970) 4161–4163, <https://doi.org/10.1021/j100717a029>.
- [54] K. Fukui, The path of chemical reactions - the irc approach, *Acc. Chem. Res.* 14 (12) (1981) 363–368, <https://doi.org/10.1021/ar00072a001>.

- [55] H. P. Hratchian, H. B. Schlegel, Following reaction pathways using a damped classical trajectory algorithm, *J. Phys. Chem. A* 106 (1) (2002) 165–169, <https://doi.org/10.1021/jp012125b>.
- [56] K. Momma, F. Izumi, *VESTA3* for three-dimensional visualization of crystal, volumetric and morphology data, *J. Appl. Crystallogr.* 44 (6) (2011) 1272–1276, <https://doi.org/10.1107/S0021889811038970>.
- [57] Marvin for javascript, <https://marvinjs-demo.chemaxon.com> (2022).
- [58] P. H. Hintermeier, S. Eckstein, D. Mei, M. V. Olarte, D. M. Camaioni, E. Baráth, J. A. Lercher, Hydronium-ion-catalyzed elimination pathways of substituted cyclohexanols in zeolite H-ZSM5, *ACS Catal.* 7 (11) (2017) 7822–7829, <https://doi.org/10.1021/acscatal.7b01582>.
- [59] L. Milakovic, P. H. Hintermeier, Q. Liu, H. Shi, Y. Liu, E. Baráth, J. A. Lercher, Towards understanding and predicting the hydronium ion catalyzed dehydration of cyclic-primary, secondary and tertiary alcohols, *J. Catal.* 390 (2020) 237–243, <https://doi.org/10.1016/j.jcat.2020.08.009>.
- [60] J. F. Bunnett, Olefin-forming elimination reactions, in: A. F. Scott (Ed.), *Survey of Progress in Chemistry*, Vol. 5 of *Survey of Progress in Chemistry*, Elsevier, 1969, pp. 53–93, <https://doi.org/10.1016/B978-0-12-395706-1.50008-X>.
- [61] F. A. Carey, R. J. Sundberg, *Advanced organic chemistry. Part. A: Structure and mechanisms*, fifth edition Edition, Springer, New York, 2007.
- [62] K. Larmier, C. Chizallet, N. Cadran, S. Maury, J. Abboud, A.-F. Lamic-Humblot, E. Marceau, H. Lauron-Pernot, Mechanistic investigation of isopropanol conversion on alumina catalysts: Location of active sites for alkene/ether production, *ACS Catal.* 5 (7) (2015) 4423–4437, <https://doi.org/10.1021/acscatal.5b00723>.
- [63] K. Larmier, C. Chizallet, S. Maury, N. Cadran, J. Abboud, A.-F. Lamic-Humblot, E. Marceau, H. Lauron-Pernot, Isopropanol dehydration on

- amorphous silica–alumina: Synergy of Brønsted and Lewis acidities at pseudo-bridging silanols, *Angew. Chem. Int. Ed.* 56 (1) (2017) 230–234, <https://doi.org/10.1002/anie.201609494>.
- [64] C. De Grotthuss, Theory of decomposition of liquids by electrical currents, *Ann. Chim* 58 (1806) 54–74.
- [65] N. Agmon, The Grotthuss mechanism, *Chem. Phys. Lett.* 244 (5) (1995) 456–462, [https://doi.org/10.1016/0009-2614\(95\)00905-J](https://doi.org/10.1016/0009-2614(95)00905-J).
- [66] J. H. Kwak, R. Rousseau, D. Mei, C. H. F. Peden, J. Szanyi, The origin of regioselectivity in 2-butanol dehydration on solid acid catalysts, *ChemCatChem* 3 (10) (2011) 1557–1561, <https://doi.org/10.1002/cctc.201100173>.
- [67] B. Chehaibou, M. Badawi, T. Bučko, T. Bazhurov, D. Rocca, Computing RPA adsorption enthalpies by machine learning thermodynamic perturbation theory, *J. Chem. Theory Comput.* 15 (11) (2019) 6333–6342, <https://doi.org/10.1021/acs.jctc.9b00782>.
- [68] T. Bučko, M. Gešvandtnerová, D. Rocca, Ab initio free energy calculations at multiple electronic structure levels made affordable: An effective combination of perturbation theory and machine learning, *J. Chem. Theory Comput.* 16 (10) (2020) 6049–6060, <https://doi.org/10.1021/acs.jctc.0c00486>.
- [69] M. Gešvandtnerová, D. Rocca, T. Bučko, Methanol carbonylation over acid mordenite: Insights from ab initio molecular dynamics and machine learning thermodynamic perturbation theory, *J. Catal.* 396 (2021) 166–178, <https://doi.org/10.1016/j.jcat.2021.02.011>.
- [70] B. Herzog, M. Chagas da Silva, B. Casier, M. Badawi, F. Pascale, T. Bučko, S. Lebègue, D. Rocca, Assessing the accuracy of machine learning thermodynamic perturbation theory: Density functional the-

- ory and beyond, *J. Chem. Theory and Comput.* 18 (3) (2022) 1382–1394, <https://doi.org/10.1021/acs.jctc.1c01034>.
- [71] A. T. Smith, P. N. Plessow, F. Studt, Density functional theory calculations of diffusion barriers of organic molecules through the 8-ring of h-ssz-13, *Chem. Phys.* 541 (2021) 111033, <https://doi.org/10.1016/j.chemphys.2020.111033>.
- [72] C. Chizallet, Toward the atomic scale simulation of intricate acidic aluminosilicate catalysts, *ACS Catal.* 10 (2020) 5579–5601, <https://doi.org/10.1021/acscatal.0c01136>.
- [73] T. Bucko, L. Benco, T. Demuth, J. Hafner, Ab initio density functional investigation of the (001) surface of mordenite, *J. Chem. Phys.* 117 (15) (2002) 7295–7305, <https://doi.org/10.1063/1.1507102>.
- [74] L. Treps, A. Gomez, T. de Bruin, C. Chizallet, Environment, stability and acidity of external surface sites of silicalite-1 and zsm-5 micro- and nano-slabs, -sheets and -crystals, *ACS Catal.* 10 (2020) 3297–3312, <https://doi.org/10.1021/acscatal.9b05103>.
- [75] J. Rey, P. Raybaud, C. Chizallet, Ab initio simulation of the acid sites at the external surface of zeolite beta, *ChemCatChem* 9 (2017) 2176–2185, <https://doi.org/10.1002/cctc.201700080>.

Table 1: Free energies ( $\Delta G$ ), enthalpies ( $\Delta H$ ), entropies ( $\Delta S$ ), and electronic contributions to free energies ( $\Delta G_{el}$ ) of relaxed reactant (R), transition state (TS) and product (P) structures of elementary reaction steps at 500 K. All values are referenced to the state with isobutanol in the gas phase and clean CHA. Bold font is used to distinguish the alcohol to alkene from other transformations.

Step	State	$\Delta G$ (kJ mol <sup>-1</sup> )	$\Delta H$ (kJ mol <sup>-1</sup> )	$\Delta S$ (J mol <sup>-1</sup> K <sup>-1</sup> )	$\Delta G_{el}$ (kJ mol <sup>-1</sup> )
<b>DH1</b>	R	-39.5	-146.5	-214	-147.0
	TS	94.0	-7.0	-202	1.5
	P	-14.0	-91.0	-155	-92.0
<b>DH2</b>	R	-60.5	-170.0	-219	-167.5
	TS	8.5	-79.5	-177	-71.5
	P	-60.0	-133.0	-146	-128.0
<b>DH3-cis</b>	R	-29.0	-136.5	-216	-138.0
	TS	53.0	-42.0	-189	-32.5
	P	-9.5	-81.5	-145	-83.5
<b>DH3-trans</b>	R	-27.0	-137.5	-222	-139.5
	TS	46.5	-44.5	-183	-36.0
	P	-12.5	-85.0	-145	-86.0
<b>DH4</b>	R	-46.5	-153.5	-215	-153.5
	TS	52.0	-41.5	-187	-31.5
	P	1.5	-67.5	-138	-69.5
<b>DH5</b>	R	-26.5	-138.0	-224	-140.0
	TS	91.0	-8.5	-199	2.0
	P	4.5	-65.0	-139	-67.5
<b>DH5w</b>	R	-34.0	-143.5	-220	-145.0
	TS	100.0	12.0	-177	18.5
	P	-38.5	-115.0	-153	-112.0

I1	R	-33.5	-144.5	-223	-146.0
	TS	82.5	-8.0	-182	-1.0
	P	-61.5	-170.0	-217	-167.5
I2	R	-32.5	-136.5	-209	-139.5
	TS	93.0	6.5	-172	8.0
	P	-59.5	-153.0	-187	-153.0
<b>DHI1-cis</b>	R	-32.5	-130.5	-196	-132.5
	TS	91.0	20.5	-141	28.0
	P	-5.5	-81.0	-151	-82.5
<b>DHI1-trans</b>	R	-25.5	-133.5	-217	-135.5
	TS	107.5	24.5	-167	32.0
	P	-10.0	-83.5	-147	-85.0
<b>DHI2</b>	R	-46.0	-151.5	-211	-152.0
	TS	98.5	8.5	-180	10.0
	P	-31.5	-103.0	-144	-101.0
DHA1-a	R	44.5	-64.5	-219	-71.5
	TS	107.5	-6.0	-227	-9.0
	P	70.5	-37.5	-217	-47.5
DHA1-b	R	50.0	-52.0	-204	-60.5
	TS	131.0	16.0	-230	21.0
	P	-33.5	-121.0	-175	-115.0
IA2-a	R	28.5	-81.0	-218	-89.5
	TS	96.0	12.5	-167	13.5
	P	32.5	-64.5	-194	-74.0
IA2-b-cis	R	52.5	-38.5	-182	-47.0
	TS	81.0	-15.0	-191	-7.0
	P	-58.5	-129.0	-141	-124.5
IA2-b-trans	R	31.5	-64.5	-192	-73.5
	TS	94.5	-5.0	-199	1.0

	P	-54.5	-131.5	-155	-128.5
IA3-b	R	22.0	-69.5	-184	-78.5
	TS	69.5	-24.5	-188	-19.0
	P	-39.5	-119.5	-160	-115.5
DHA5	R	45.5	-72.0	-235	-79.5
	TS	124.5	23.0	-203	16.0
	P	19.5	-72.0	-183	-81.0

Table 2: Free energies of activation ( $\Delta G^\ddagger$ ), enthalpies of activation ( $\Delta H^\ddagger$ ), entropies of activation ( $\Delta S^\ddagger$ ), and electronic contributions to free energies of activation ( $\Delta G_{el}^\ddagger$ ) for elementary reaction steps at 500 K.

Transformation	Step	$\Delta G^\ddagger$ (kJ mol <sup>-1</sup> )	$\Delta H^\ddagger$ (kJ mol <sup>-1</sup> )	$\Delta S^\ddagger$ (J mol <sup>-1</sup> K <sup>-1</sup> )	$\Delta G_{el}^\ddagger$ (kJ mol <sup>-1</sup> )
Alcohol to Alkene	DH1	133.5	139.5	12	148.5
	DH2	69.0	90.0	43	96.0
	DH3-cis	81.5	94.5	26	105.5
	DH3-trans	73.5	93.0	39	103.5
	DH4	98.5	112.0	28	122.0
	DH5	117.5	130.0	25	142.0
	DH5w	134.0	155.5	43	163.5
	DHI1-cis	123.5	151.5	55	161.0
	DHI1-trans	133.0	158.0	50	167.5
	DHI2	144.5	160.0	31	162.5
Alcohol to Alcohol	I1	116.0	136.5	41	145.0
	I2	125.0	143.5	36	147.0

Table 3: Free energies of reaction ( $\Delta G_{R \rightarrow P}$ ), enthalpies of reaction ( $\Delta H_{R \rightarrow P}$ ), entropies of reaction ( $\Delta S_{R \rightarrow P}$ ), and electronic contributions to the free energies of reaction ( $\Delta G_{el,R \rightarrow P}$ ) of elementary reaction steps at 500 K.

Transformation	Path	$\Delta G_{R \rightarrow P}$ (kJ mol <sup>-1</sup> )	$\Delta H_{R \rightarrow P}$ (kJ mol <sup>-1</sup> )	$\Delta S_{R \rightarrow P}$ (J mol <sup>-1</sup> K <sup>-1</sup> )	$\Delta G_{el,R \rightarrow P}$ (kJ mol <sup>-1</sup> )
Alcohol to Alkene	DH1	26.0	55.5	60	55.0
	DH2	0.5	37.0	73	39.5
	DH3-cis	19.5	55.0	71	54.5
	DH3-trans	14.5	52.5	77	53.0
	DH4	48.0	86.5	77	84.0
	DH5	31.0	73.5	85	72.5
	DH5w	-4.5	28.5	67	33.5
	DHI1-cis	27.0	49.5	45	50.0
	DHI1-trans	15.0	50.5	70	50.5
	DHI2	15.0	48.5	67	51.0
Alcohol to Alcohol	I1	-28.0	-25.0	5	-21.5
	I2	-27.0	-16.5	22	-13.5

Table 4: Selected interatomic distances in transition states (see Fig. 4). All distances are in Å.

Path	d <sub>1</sub>	d <sub>2</sub>	d <sub>3</sub>	d <sub>4</sub>	d <sub>5</sub>	d <sub>6</sub>	d <sub>7</sub>
DH1	2.335	1.517	-	-	-	-	-
DH2	2.920	2.864	-	-	-	-	-
DH3-cis	2.595	1.545	-	-	-	-	-
DH3-trans	2.536	1.533	-	-	-	-	-
DH4	2.564	1.418	-	-	-	-	-
DH5	2.310	1.386	-	-	-	-	-
DH5w	2.552	-	-	-	-	1.432	1.250
DHI2	2.592	3.489	-	1.749	1.832	-	-
DHI1-cis	2.460	2.595	-	-	-	1.370	1.292
DHI1-trans	2.450	2.187	-	-	-	1.377	1.292
I1	2.314	-	3.123	-	-	1.318	1.344
I2	2.521	-	2.979	1.754	1.853	-	-

Table 5: The energy spans ( $\Delta G_{ES}$ ) calculated for different isobutanol to butenes transformation routes at  $T = 500$  K.

Product	Steps	Path	$\Delta G_{ES}$ (kJ mol <sup>-1</sup> )
Isobutene	1	DH1	133.5
	2	I1, DH2	116.0
	5	R-a, R-b, R-c, DHA1-a, DHA1-b	170.5
<i>Cis</i> -but-2-ene	4	DH1, -DHA1-b, IA2-a, IA2-b-cis	170.5
	2	I2, DH3-cis	125.0
	6	R-a, R-b, R-c, DHA1-a, IA2-a, IA2-b-cis	147.0
<i>Trans</i> -but-2-ene	4	DH1, -DHA1-b, IA2-a, IA2-b-trans	170.5
	2	I2, DH3-trans	125.0
	6	R-a, R-b, R-c, DHA1-a, IA2-a, IA2-b-trans	147.0
But-1-ene	4	DH1, -DHA1-b, IA2-a, IA3-b	170.5
	1	DH12	144.5
	2	I2, DH4	128.5
	6	R-a, R-b, R-c, DHA1-a, IA2-a, IA3-b	147.0

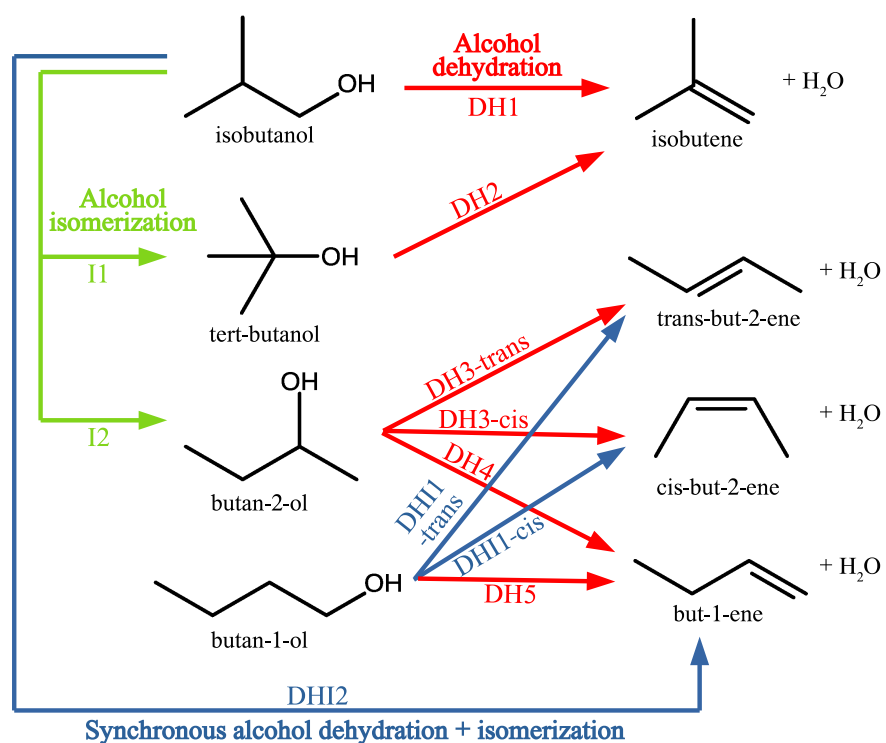


Figure 1: Reaction network of monomolecular alcohol transformations into butenes via free cationic species. The path labelling shown in the scheme is used throughout this document. The color code depicts the type of reaction as follows: red: alcohol dehydration (paths DH1-5), green: alcohol isomerization (paths I1-2), and blue: synchronous alcohol dehydration plus isomerization (paths DHI1-2).

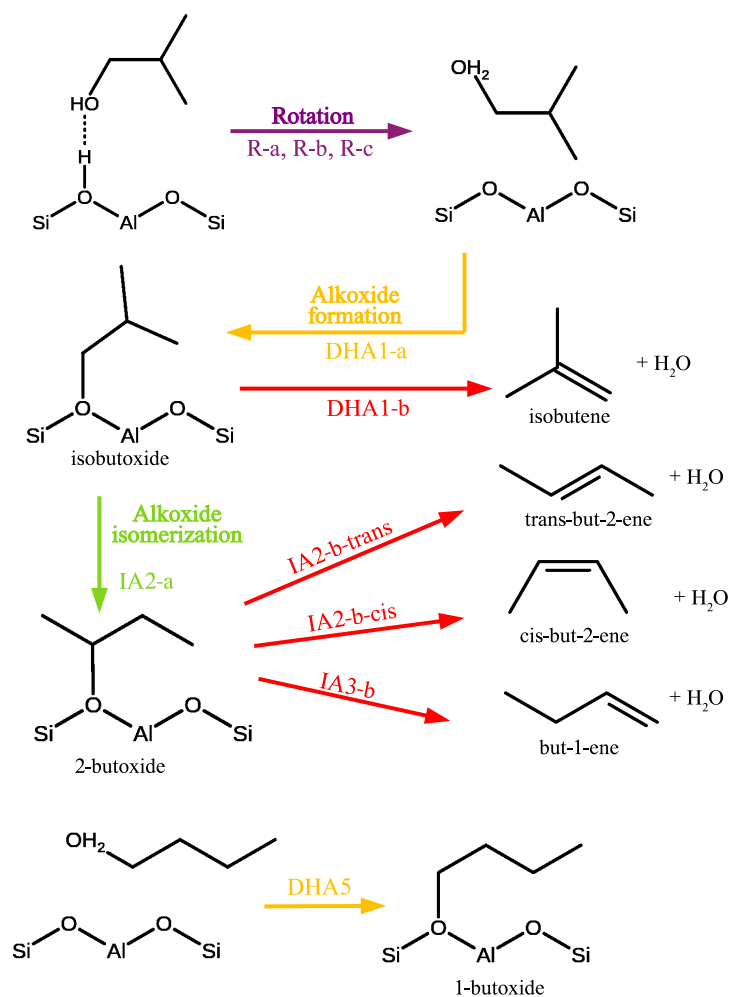


Figure 2: Reaction network of transformations of isobutanol to butenes via alkoxide intermediates. The path labelling shown in the scheme is used throughout this work. The color code depicts the type of reaction as follows: purple: isobutanol rotation (paths R-a, R-b, and R-c), orange: formation of alkoxide intermediate from alcohol (paths DHA1-a, and DHA5), green: alkoxide isomerization (path IA2-a), red: alkoxide to alkene transformations (paths DHA1-b, IA2-b-cis, IA2-b-trans, and IA3-b).

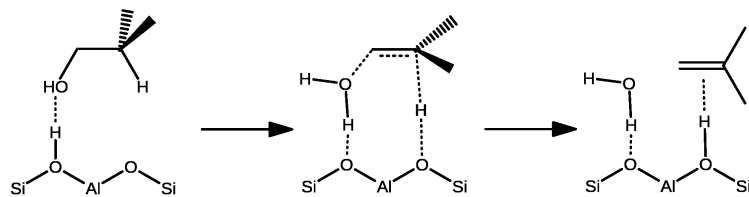


Figure 3: Schematic representation of mechanism identified by IRC procedure for transformation of isobutanol to isobutene (path DH1).

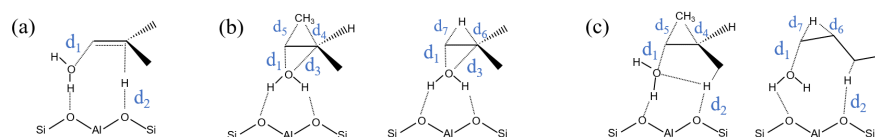


Figure 4: Schematic representation of selected transition states structures with labelling of the distances reported in table 4. (a) E2 dehydration reaction (DH), (b) alcohol isomerization (I), (c) synchronous dehydration and isomerization (DHI). A single example is given in each case, but distances are defined generally for all alcohols as follows:  $d_1$ : O (from OH) ... C (on carbenium from which protonated OH disconnects),  $d_2$ : H (on carbenium) ... O (either on water or zeolitic active site, to which the carbenium cation deprotonates),  $d_3$ : O (from OH) ... C (on carbenium to which OH connects),  $d_4$ : C (from carbenium from which  $\text{CH}_3$  shifts) ... C (from  $\text{CH}_3$ ),  $d_5$ : C (from carbenium to which  $\text{CH}_3$  shifts) ... C (from  $\text{CH}_3$ ),  $d_6$ : C (from which H shifts) ... H, and  $d_7$ : C (to which H shifts) ... H.

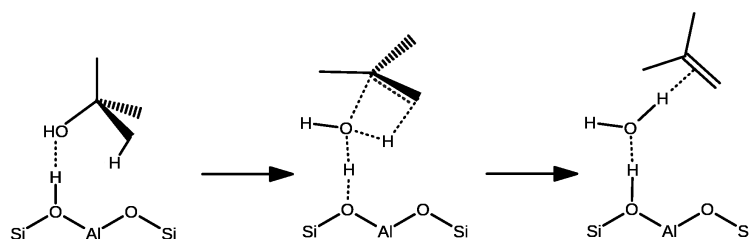


Figure 5: Schematic representation of mechanism identified by IRC procedure for the transformation of tert-butanol to isobutene (path DH2) mediated by  $\text{H}_2\text{O}$ .

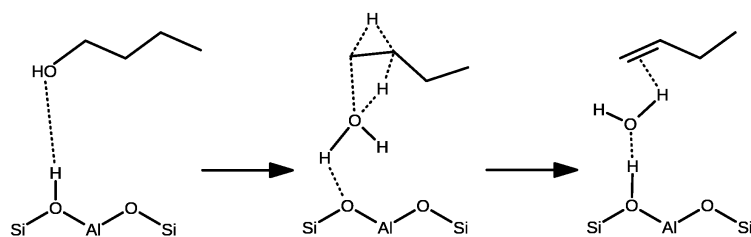


Figure 6: Schematic representations of mechanism identified by IRC procedure for the dehydration of butan-1-ol to but-1-ene towards a water mediated mechanism combined with hydride shift (path DH5w).

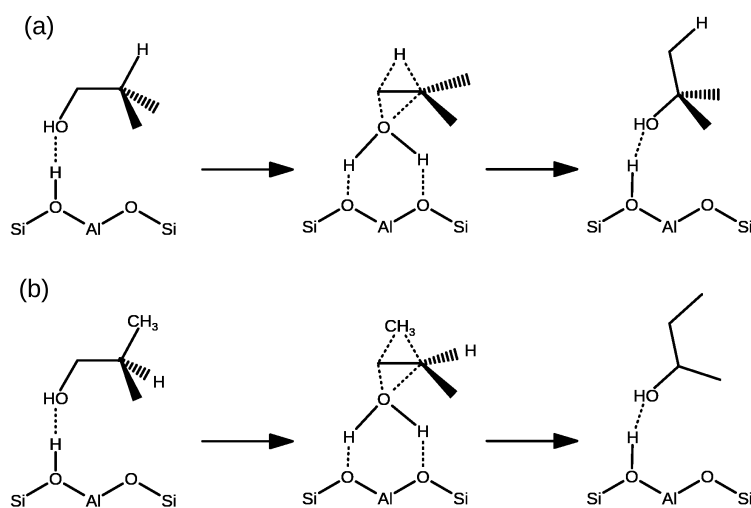


Figure 7: Schematic representation of mechanism identified by IRC procedure for transformation of isobutanol to tert-butanol (a: path I1), and isobutanol to butan-2-ol (b: path I2).

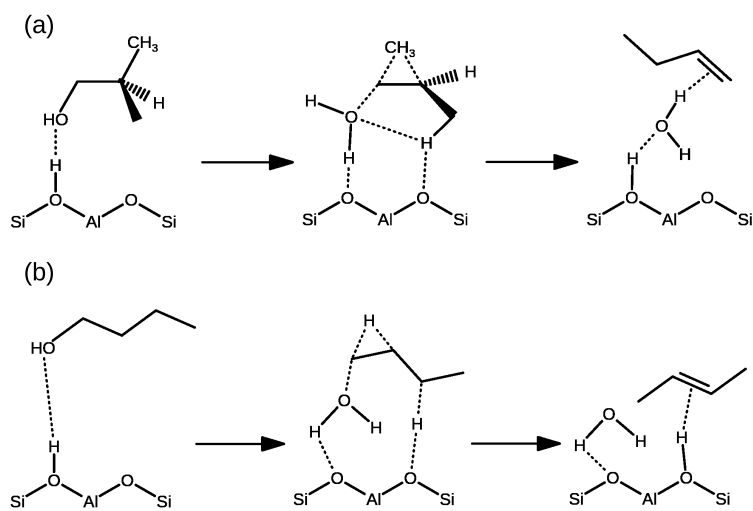


Figure 8: Schematic representations of mechanisms identified by IRC procedure for transformation of isobutanol to but-1-ene (a: path DHI2), and butan-1-ol to but-2-ene (b: path DHI1, here DHI1-trans is illustrated).

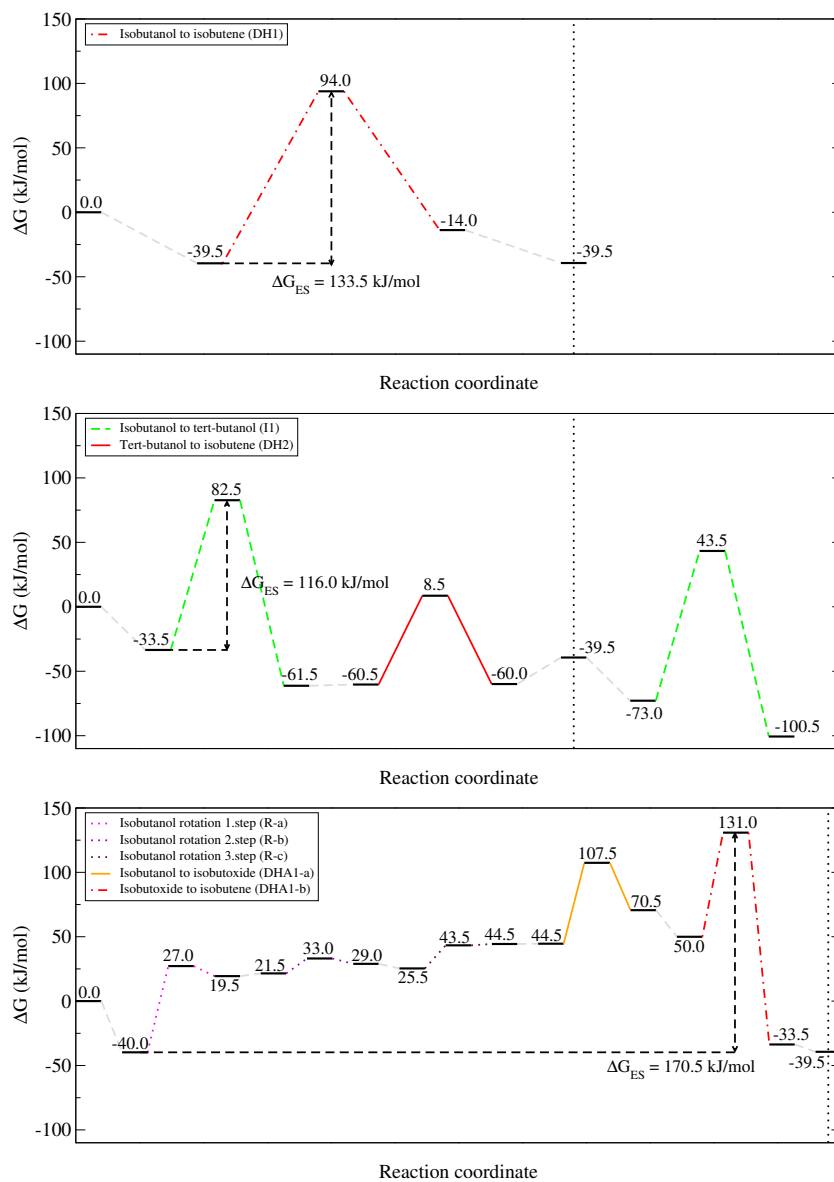


Figure 9: Free energy profiles for the transformation of isobutanol to isobutene at  $T=500$  K proceeding via a one step mechanism (path DH1), via mechanism involving tert-butanol intermediate (path I1 and DH2), and via mechanism involving isobutoxide intermediate (paths R-a, R-b, R-c, DHA1-a, DHA1-b). The beginning of the second catalytic cycle is indicated by a vertical dotted line. Energy span ( $\Delta G_{ES}$ ) of each reaction is highlighted by dashed arrows.

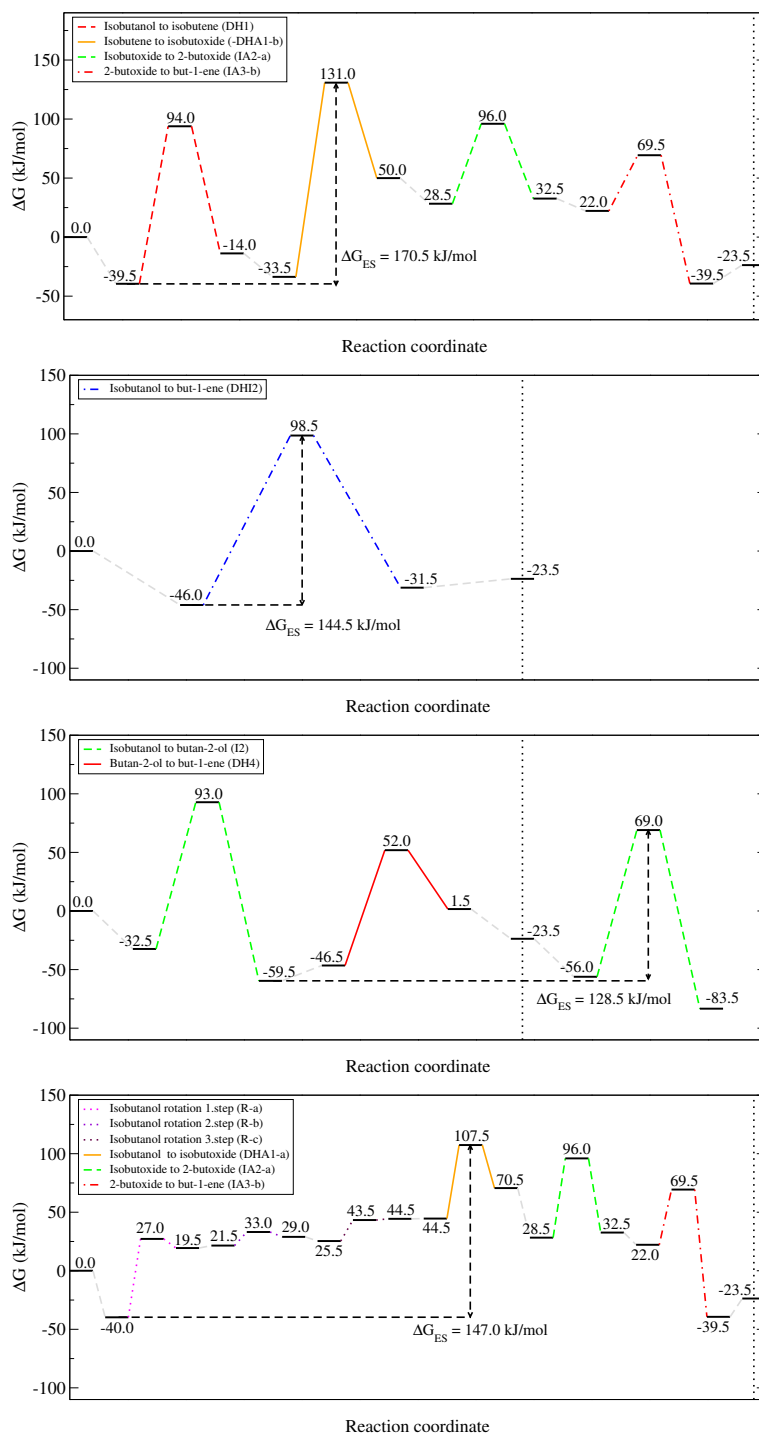


Figure 10: Free energy profiles for the transformation of isobutanol to but-1-ene at  $T=500$  K proceeding via isobutene isomerization (paths DH1, DHA1-b, IA2-a, IA3-b), via one step mechanism (path DHI2), via butan-2-ol intermediate (path I2 and DH4), and via isobutoxide and secondary butoxide intermediates (paths R-a, R-b, R-c, DHA1-a, IA2-a, IA3-b). The beginning of the second catalytic cycle is indicated by a vertical dotted line. Energy span ( $\Delta G_{ES}$ ) of each reaction is highlighted by dashed arrows.

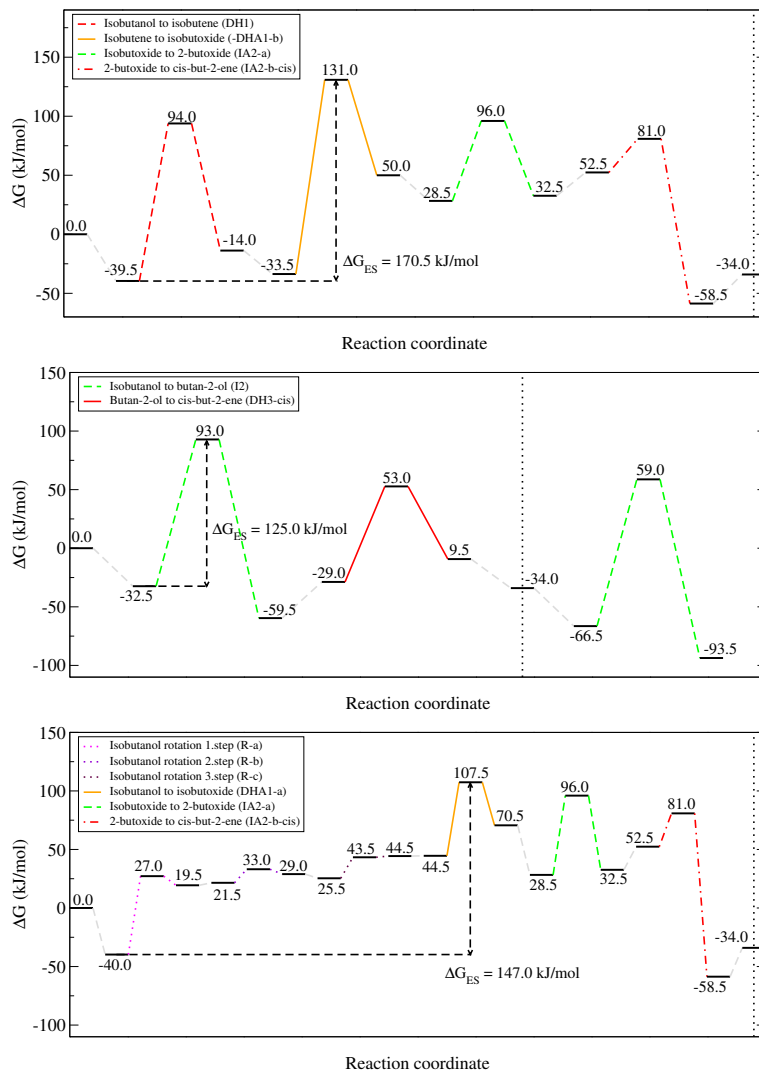


Figure 11: Free energy profiles for the transformation of isobutanol to *cis*-but-2-ene at  $T=500$  K proceeding via isobutene isomerization (paths DH1, -DHA1-b, IA2-a, IA2-b-cis), via butan-2-ol intermediate (path I2 and DH3-cis), and via isobutoxide and secondary butoxide intermediates involving three step rotation of isobutanol (paths R-a, R-b, R-c, DHA1-a, IA2-a, IA2-b-cis). The beginning of the second catalytic cycle is indicated by a vertical dotted line. Energy span ( $\Delta G_{ES}$ ) of each reaction is highlighted by dashed arrows.

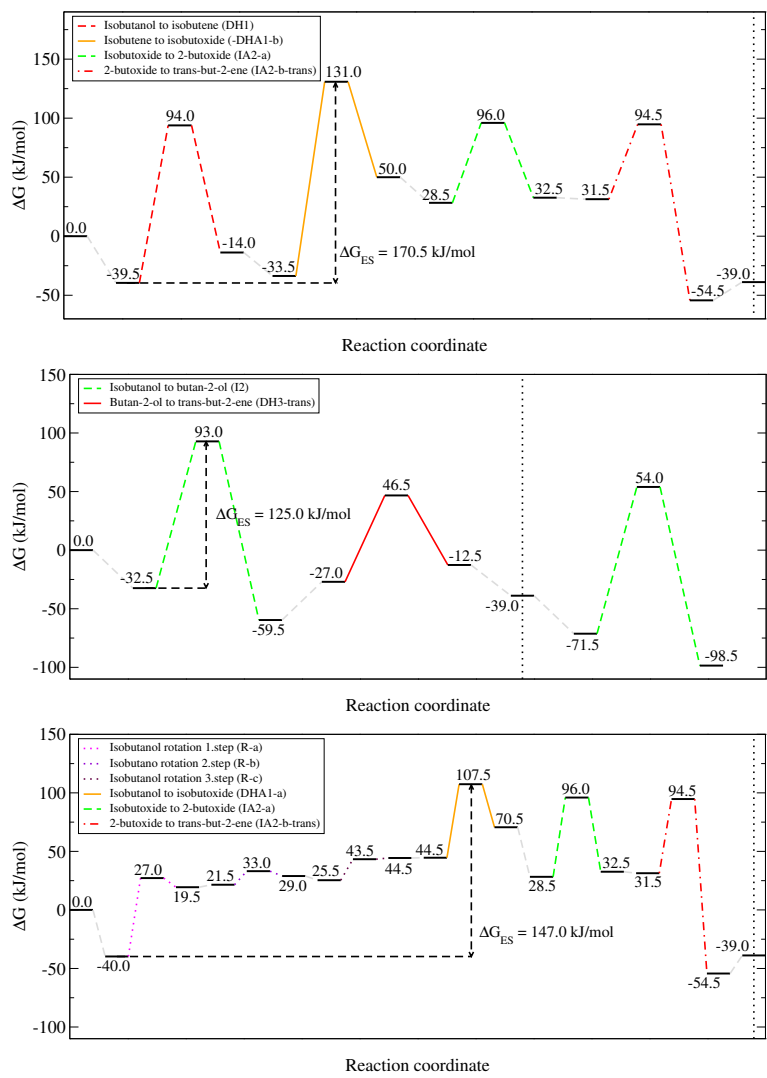


Figure 12: Free energy profiles for the transformation of isobutanol to *trans*-but-2-ene at  $T=500$  K proceeding via isobutene isomerization (paths DH1, -DHA1-b, IA2-a, IA2-b-trans), via butan-2-ol (path I2 and DH3-trans), and via isobutoxide and secondary butoxide intermediates (paths R-a, R-b, R-c, DHA1-a, IA2-a, IA2-b-trans). The beginning of the second catalytic cycle is indicated by a vertical dotted line. Energy span ( $\Delta G_{ES}$ ) of each reaction is highlighted by dashed arrows.

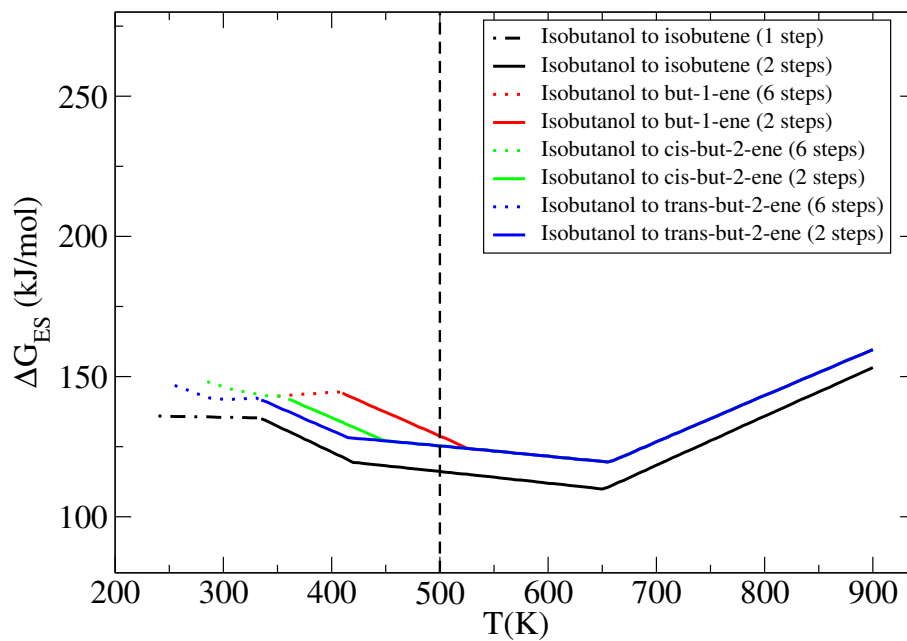


Figure 13: Temperature dependence of the energy spans ( $\Delta G_{ES}$ ) of the preferred mechanisms for transformations of isobutanol to isobutene, but-1-ene, *cis*-but-2-ene, and *trans*-but-2-ene. Vertical dashed line indicates the results obtained for the temperature of 500 K, for which free energy profiles are displayed in Fig. 9, 10, 11, and 12.